Review

A-Site Cation Chemistry in Halide Perovskites

Published as part of Chemistry of Materials virtual special issue "In Memory of Prof. Francis DiSalvo".

Matthew P. Hautzinger,* Willa Mihalyi-Koch, and Song Jin

Read Online

ACCESS | Metrics & More | Article Recommendations

ABSTRACT: Metal halide perovskites are an important class of semiconductors now being implemented as photovoltaic absorbers and explored for light emission, among other device applications. The semiconducting properties of halide perovskites are deeply intertwined with their composition and structure. Specifically the symmetry, tilting, and distortions of the metal halide octahedra impact the band structure and other optoelectronic properties. In this review, we examine the various compositions of monovalent A-site cations in three-dimensional (3D) halide perovskites AMX_3 (M = divalent metal; X = halide). We focus on how the A-site cation templates the inorganic metal-halide perovskite framework, resulting in changes in the crystal structure symmetry, as well as M−X bonding parameters,

summarized in a comprehensive table of AMX_3 structures. The A-site cation motion, effects of alloying, and 2D Ruddlesden−Popper perovskite structures with unique A-site cations are further overviewed. Correlations are shown between these A-site cation dominated structural parameters and the resulting optoelectronic properties such as band gap. This review should serve as a reference for the A-site cation structural chemistry of metal halide perovskites and inspire continued research into less explored metal halide perovskite compositions and structures.
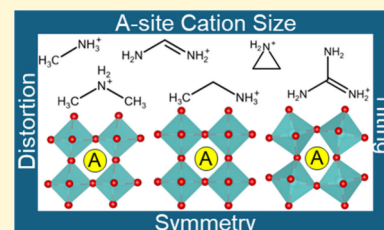
INTRODUCTION

Metal halide perovskites have numerous demonstrated semiconductor applications including high-efficiency photovoltaics (PVs),[1,2] lasing and light emitting diodes,[3,4] X-ray detectors,[5] field effect transistors,[6] and spintronic devices.[7,8] Investigation into growing metal halide perovskites in thin films, nanocrystals (NCs), and other nanostructures and has enabled these applications.[9−11] Underpinning such processing and applications are solid-state chemistry studies of the crystal structures and physical properties of halide perovskites.

The prototypical three-dimensional (3D) halide perovskite structure AMX_3 [A = monovalent cation; M = Pb^{2+}, Sn^{2+}, Ge^{2+}; and X = I^-, Br^-, Cl^-] is a corner sharing network of MX_6^{4-} octahedra with an A-site cation occupying the 12-coordinate cavity formed by eight octahedra (Figure 1a−c), sometimes referred to as the "perovskite cage".[12] AMX_3 halide perovskites are highly tunable with a variety of combinations of metal and halide ions, and their solid solutions are accessible. By incorporating bulky ammonium cations, the 3D MX_6^{4-} octahedral network can be broken up into 2D layered perovskite variants with these bulky ammonium spacer cations between perovskite layers forming natural quantum wells (QWs), such as Ruddlesden−Popper (RP)[13,14] (Figure 1d) or Dion−Jacobson (DJ)[15] phases, with the formula $(A')_m(A)_{n-1}M_nX_{3n+1}$ (A′ = alky- or aryl-ammonium spacer cation for m = 2 RP, or diammonium cation for m = 1 DJ perovskite). The number of inorganic layers (n), i.e., the
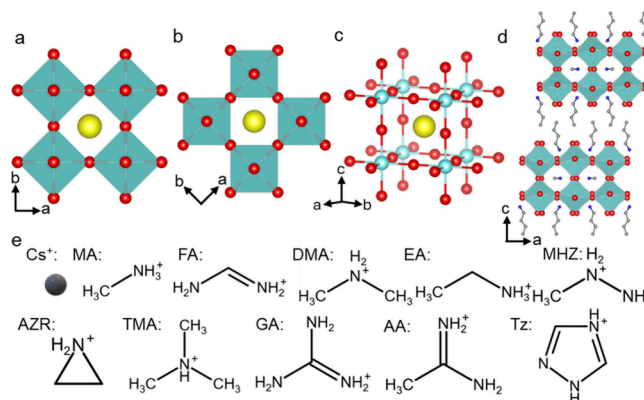
Figure 1. Common halide perovskite crystal structures and A-site cations. (a−c) Different representations of the 3D AMX_3 structure with corner sharing metal halide octahedra. (d) Crystal structures of 2D Ruddlesden−Popper (RP) perovskite (n = 2). (e) A-site cations that have been confirmed via crystallography to occupy the A-site cavity of AMX_3 or 2D $(A')_2(A)_{n-1}M_nX_{3n+1}$ halide perovskite structures. MA = methylammonium, FA = formamidinium, DMA = dimethylammonium, EA = ethylammonium, MHz = methylhydrazinium, AZR = aziridinium, TMA = trimethylammonium, Ga = guanidinium, AA = acetamidinium, and Tz = 1,2,4-triazolium.
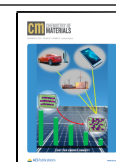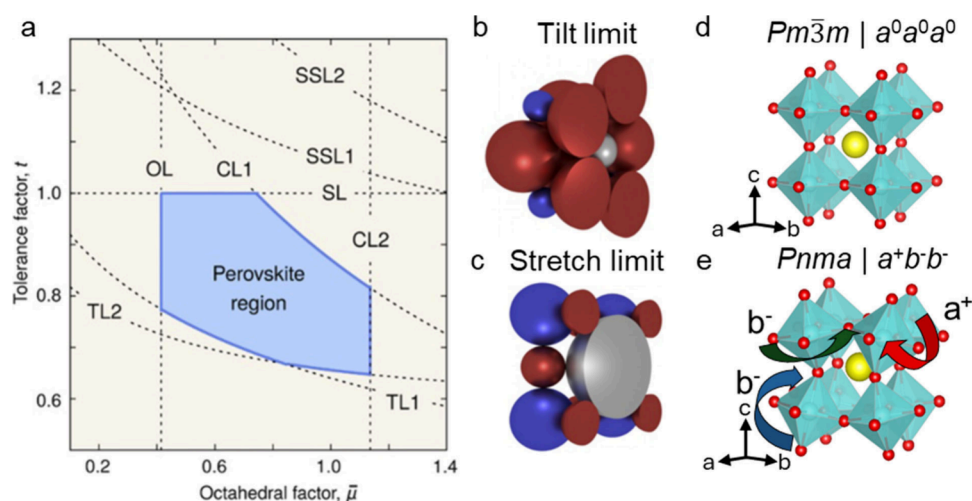
Figure 2. Description of the phase stability, octahedral tilting, and crystal symmetry in AMX$_3$ halide perovskite. (a) Plot of tolerance factor and octahedral factor showing the blue shaded stability region of 3D perovskites as well as lines delimiting the tilt limit (TL), octahedral limit (OL), chemical limit (CL), stretch limit (SL), and secondary stretch limit (SSL). Schematic of the perovskite structures at the (b) tilt limit and the (c) stretch limit (silver = A-site cations, blue = B cations, and red = X anions). Representative structure diagram (d) of an $a^0a^0a^0$ perovskite structure lacking octahedral tilting and an $a^+b^-b^-$ structure (e) with tilting along the a axis (a^+) in a different direction and lesser extent than the b and c axis tilting (b^-). Panels a, b, and c reproduced from *Proc. Natl. Acad. Sci.* **2018**, *115* (21), 5397−5402.[22]

---

thickness of the QWs, is controlled by the ratio of A-site and A′ cations.

The composition of the halide perovskite dictates the crystal symmetry, distortion of the perovskite framework, and the ability to form a stable perovskite. This in turn determines the optoelectronic properties. While several recent reviews have summarized the developments in the general structural chemistry and spacer cation tuning of 2D halide perovskites,[16−19] the materials chemistry of A-site cations in 3D AMX$_3$ perovskites has not been systematically surveyed from a solid-state chemistry point of view. In this Review, we will examine the role of the A-site cation in templating the inorganic framework through a comprehensive summary of the AMX$_3$ crystal structures including the crystal symmetry, tilting of octahedra, and structural distortions. Select works on A-site cation motion and alloying of A-site cations will be discussed in the context of structural chemistry. We will also discuss the effect of A-site cations on higher n-value RP perovskites, specifically focusing on unique A-site cations that are not possible to incorporate in the 3D AMX$_3$ phase. The relationship between the band gap energy and A-site cation is discussed as a proxy for how the A-site cation can impact the AMX$_3$ structure.

Description of Structural Tolerance Factor, Octahedral Tilting, and Distortions in Halide Perovskites. Empirical models based on bonding and ionic radii have been developed to predict a perovskites' ability to form.[20−24] Relative to the traditional highly ionic oxide perovskites, the M−X bonds in halide perovskites are more covalent in nature.[23,24] The empirical Goldschmidt tolerance factor (α) defined in eq 1 was originally used for highly ionic oxide perovskites and can be applied to the more covalent halide perovskites as a rule of thumb for whether a perovskite will form with a specific compsition.

$$\alpha = \frac{r_a + r_x}{\sqrt{2}\,(r_M + r_x)} \tag{1}$$

r_i is the radii of the various ions in AMX$_3$ (i = A, M, X). To determine r_a for the nonspherical organic cations, an effective

ionic radius is calculated as the distance between the center of mass of the molecule to the furthest atom, added to the radius of that atom.[21] In addition, the octahedral factor (μ) defined in eq 2 is used to predict the preferential formation of individual MX$_6$ octahedra versus other geometries. The octahedral limit describes when the B metal is too small or large relative to the anions, resulting in formation of a different geometry such as a tetrahedron.

$$\mu = \frac{r_M}{r_x} \tag{2}$$

Goldschmidt's no-rattling principle dictates that α and μ must be within empirically defined limits for a stable perovskite to form, as shown in the plot of tolerance factor vs octahedral factor in Figure 2a.[22]

The size of the A-site cation plays a large role in dictating octahedral tilting.[22] Under the tilt limit, the A-site cation is small, leaving a void for the octahedra to tilt at moderate α and promoting a nonperovskite structure when $\alpha < 0.8$ (Figure 2b). In contrast, under the stretch limit where $\alpha > 1$, the A-site cation is too large, stretching the M−X distances beyond what forms stable perovskites (Figure 2c). The structural symmetry is dictated by the type and degree of tilting of the octahedra. As described by the Glazer notation (e.g., $a^0b^+c^-$), MX$_6$ octahedra can tilt in the same direction (in-phase) or opposite direction (antiphase) or have no tilt, which is indicated along different crystallographic axis as superscripts +, −, and 0, respectively.[25] Furthermore, the octahedra can have the same or unique amplitude of tilt, indicated by *a a a* for the same amplitude or *a b c* for each amplitude of tilt independent along unique crystallographic directions (ref 25 for complete description). For example, $a^0a^0a^0$ has no tilting (Figure 2d) and adopts the $Pm\bar{3}m$ space group. In contrast, Figure 2e shows an $a^+b^-b^-$ structure which has tilting about each axis, with the b and c axis the same degree of tilt, and fits into the lower symmetry $Pnma$ space group.[26]

Another consideration is the individual MX$_6$ octahedra, which can be distorted with deviations from the ideal M−X lengths and X−M−X bond angles. The bond length distortion
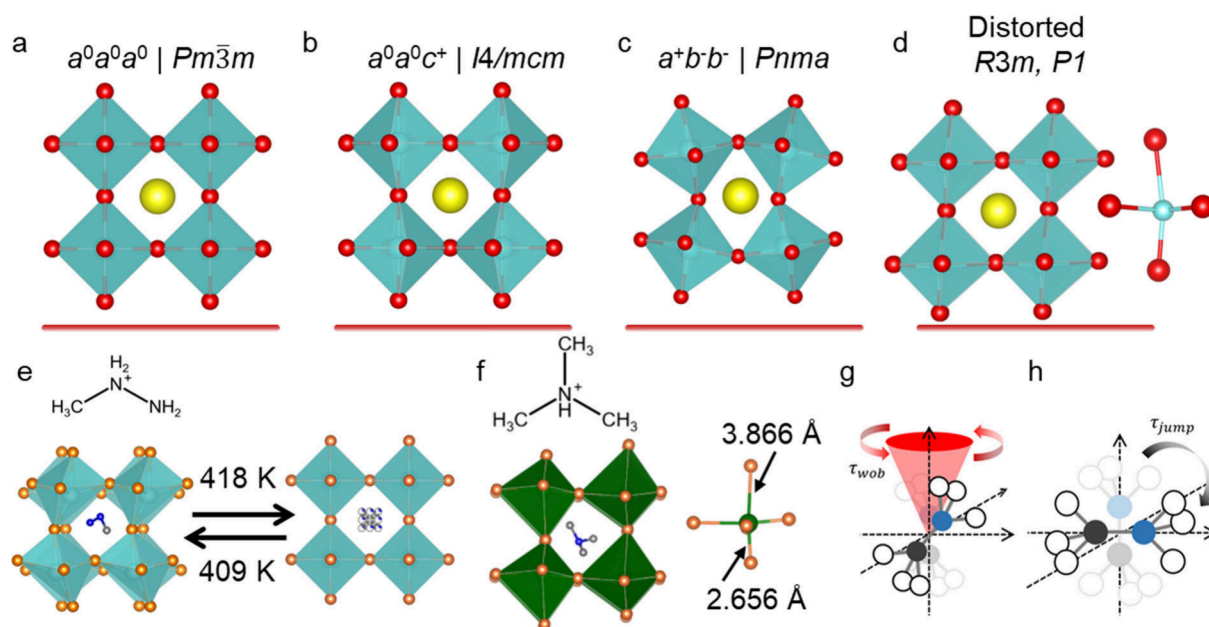
Figure 3. Range of halide perovskite structures from ideal to increasingly distorted, those with exotic A-site cations, and illustration of cation reorientations. (a) Ideal $Pm\bar{3}m$ perovskite structure with no tilting or distortion of the octahedra. (b) Octahedra slightly tilted along one axis due to the smaller ratio of A-cation size to MX_6 (lower α). (c) Tilted perovskite where each axis is tilted. (d) Perovskite structure with distorted octahedra and an individual octahedron highlighted on the right. (e) The methylhydrazinium (MHz) cation found in the RT noncentrosymmetric $P2_1$ and high temperature $Pm\bar{3}m$ structures of $(MHz)PbBr_3$.[29] (f) Trimethylammonium (TMA) cation and the $(TMA)SnBr_3$ structure.[30,31] The distortions and off-centering of Sn^{2+} can be clearly seen in the individual octahedron highlighted on the right. Diagrams illustrating the (g) wobbling rotations of MA cations and the (h) jump reorientation.[32] Panels g and h are reproduced or adapted with permission from ref 32. Copyright 2018 American Chemical Society.

index (D) describes the elongation of the M−X bond lengths (d_i) relative to ideal M−X bond lengths (d_0) in eq 3:[27]

$$D = \frac{1}{6} \sum_{i=1}^{6} \frac{|d_i - d_0|}{d_0} \tag{3}$$

The X−M−X bond angle (θ_i) distortion can be described with the bond angle variance (σ^2):[28]

$$\sigma^2 = \frac{1}{11} \sum_{i=1}^{12} (\theta_i - 90)^2 \tag{4}$$

The combination of D and σ^2 captures the various distortions in an octahedron, which in turn alter the symmetry of the overall structure.

Effect of A-Site Cations on the 3D Perovskite Structures. Halide perovskites form four common crystal structure types at room temperature (RT) depicted in Figure 3a−d depending on the interplay of ionic radius sizes among the A-site cation, metal, and halide. AMX_3 compounds with crystal structures determined and their tolerance factors, symmetries, bonding parameters, and band gap of each compound are summarized in Table 1.

Most MA based perovskite compounds $(MA)PbX_3$ (X = Cl, Br)[38,40,55] and $(MA)SnX_3$[44,47] have favorable tolerance factors (Table 1) and as a result form the $a^0a^0a^0$ $Pm\bar{3}m$ structures (Figure 3a) which are examples of ideal, high symmetry perovskite structures. MA cations form two other perovskite structures with Pb and Sn that tilt and deviate from ideal structures: $(MA)PbI_3$ has been reported in the $Fmmm$,[38] $I4/m$,[56] $I4/mcm$,[34,57,58] and $I4cm$[12] space groups. Twinning in these crystals presents a challenge in assigning the space group via single crystal X-ray diffraction.[38] Rotational SHG measure-

ments which map the symmetry of the structure suggest bulk $(MA)PbI_3$ likely adopts the $I4/mcm$ space group.[57] $(MA)PbI_3$ has a slightly tilted structure described as $a^0a^0c^-$ (Figure 3b). The slight tilting along a single axis correlates with an α value of 0.91 in the middle of the other halide perovskites. In contrast, $(MA)SnI_3$ adopts the $Pm\bar{3}m$ space group ($a^0a^0a^0$) since α is larger (0.95), pushing it closer to the stretch limit and thus having no tilting. The other nonideal MA based halide perovskite is $(MA)SnCl_3$ ($P1$, Figure 3d),[50] which can be described as a distorted perovskite with large σ^2 and D values (Table 1). We can deduce that the lone pair of Sn^{2+} ($5s^2$)[46] in combination with the short Cl bonds cause the distortions in the $(MA)SnCl_3$ structure, not predicted by the α and μ.[59]

The slightly larger formamidinium (FA) cation forms $(FA)PbX_3$ (X = Cl, Br) and $(FA)SnX_3$ (X = Br, I) perovskite structures in the $Pm\bar{3}m$ space group with no tilts ($a^0a^0a^0$).[39,41,45,60] These structures all form halide perovskites in spite of having a slightly unfavorable $\alpha > 1$ (Table 1), which demonstrates the empirical nature of α. However, $(FA)MI_3$ (M = Sn, Pb) that have α close to 1 are a metastable perovskite phase ($Pm\bar{3}m$, $a^0a^0a^0$) at room temperature.[35,61,62] Under ambient conditions, $(FA)PbI_3$ converts to a thermodynamically stable nonperovskite yellow phase, indicating the structural instability of these compounds.[61] FA based perovskites are an excellent example of halide perovskites existing at the stretch limit, where the large FA cation causes MX_6 octahedra in the structure to adopt the $Pm\bar{3}m$, $a^0a^0a^0$ structure with no tilting.

Cs^+ is the primary alkali A-site cation found in the crystal structures of inorganic halide perovskites, although solid solutions containing Rb^+ have been reported.[37,63] At RT, $CsPbX_3$ (X = Cl, Br) forms a tilted structure in the $Pbnm$ (no.

Table 1. Tolerance Factor (α), Select Crystal Structure Parameters, and Band Gap for Each Reported 3D Perovskite Structure[a]

Compound	α	Space group (RT)	Tilt	D	σ^2	Avg. Bond Length (Å)	Unit Cell Vol./Z (Å³)	Band gap (eV)
CsPbI$_3$[33]	0.851	$Pnam$	$a^+b^-b^-$	0.0092	2.5422	3.1773	236.83	1.72
(MA)PbI$_3$[34]	0.912	$I4/mcm$	$a^0a^0c^+$	0.0006	0	3.1522	248.64	1.51
(FA)PbI$_3$[35]	0.987	$Pm\bar{3}m$	$a^0a^0a^0$	0	0	3.181	256.9	1.41
(AZR)PbI$_3$[36]	0.932	$Pm\bar{3}m$	$a^0a^0a^0$	0	0	3.1820	257.74	1.52
CsPbBr$_3$[37]	0.862	$Pnma$	$a^+b^-b^-$	0.0006	0.5659	2.9699	200.69	2.27
(MA)PbBr$_3$[38]	0.927	$Pm\bar{3}m$	$a^0a^0a^0$	0	0	2.9664	208.82	2.23
(FA)PbBr$_3$[39]	1.01	$Pm\bar{3}m$	$a^0a^0a^0$	0	0	3.0067	217.45	2.15
(AZR)PbBr$_3$[36]	0.950	$Pm\bar{3}m$	$a^0a^0a^0$	0	0	2.9869	213.19	2.27
(MHz)PbBr$_3$[29]	1.03	$P2_1$	$a^+b^0c^0$	0.0262	301.17	3.0424	209.18	2.49
CsPbCl$_3$[37]	0.870	$Pbnm$	$a^+b^-b^-$	0.0027	0.4451	2.8309	175.52	2.91
(MA)PbCl$_3$[40]	0.938	$Pm\bar{3}m$	$a^0a^0a^0$	0	0	2.8433	182.80	2.88
(FA)PbCl$_3$[41]	1.02	$Pm\bar{3}m$	$a^0a^0a^0$	0	0	2.8689	188.91	3.00
(AZR)PbCl$_3$[36]	0.961	$Pm\bar{3}m$	$a^0a^0a^0$	0	0	2.8805	191.20	2.99
(MHz)PbCl$_3$[42]	1.05	$P2_1$	distorted	0.0242	314.38	2.9249	184.80	3.14
CsSnI$_3$[43]	0.890	$Pnam$	$a^+b^-b^-$	0.0028	21.998	3.1143	232.37	1.3
(MA)SnI$_3$[44]	0.954	$Pm\bar{3}m$	$a^0a^0a^0$	0	0	3.1217	243.37	1.21
(FA)SnI$_3$[45]	1.03	$Pm\bar{3}m$	$a^0a^0a^0$	0	0	n/a	251.19	1.41
CsSnBr$_3$[46]	0.905	$Pm\bar{3}m$	$a^0a^0a^0$	0	0	2.9021	195.55	1.9
(MA)SnBr$_3$[47]	0.973	$Pm\bar{3}m$	$a^0a^0a^0$	0	0	2.9537	206.16	2.3
(FA)SnBr$_3$[45]	1.06	$Pm\bar{3}m$	$a^0a^0a^0$	0	0	2.9931	214.51	2.63[48]
(MP)SnBr$_3$[49]	n/a	Pc	distorted	0.1079	8.6323	3.0462	215.79	2.45
(TMA)SnBr$_3$[30]	n/a	$P2_1$	distorted	0.1710	48.448	3.2144	259.42	2.76[31]
CsSnCl$_3$[50]	0.916	$Pm\bar{3}m$	$a^0a^0a^0$	0	0	2.752	166.7	2.88[48]
(MA)SnCl$_3$[50]	0.987	$P1$	distorted	0.0926	72.264	2.8286	186.04	3.5[48]
(GA)SnCl$_3$[51]	1.06	$Pbca$	distorted	0.1612	99.193	3.0191	208.65	n/a
(TMA)SnCl$_3$[31]	n/a	$Cmc2_1$	distorted	0.2061	36.117	3.1373	242.34	3.59
CsGeI$_3$[52]	1.03	$R3m$	distorted	0.0838	32.102	3.0044	213.96	1.6
(MA)GeI$_3$[52]	1.06	$R3m$	distorted	0.1083	44.875	3.1093	235.73	1.9
(FA)GeI$_3$[52]	1.14	$R3m$	distorted	0.1338	74.410	3.1551	242.72	2.3
CsGeBr$_3$[53]	0.95	$R3m$	distorted	0.103	19.83	2.825	178.8	2.38
(MA)GeBr$_3$[54]	1.09	$R3m$	distorted	0.1412	24.693	2.9112	195.24	2.91
(FA)GeBr$_3$[54]	1.18	$R3m$	distorted	0.1668	77.212	2.9971	207.42	3.13
CsGeCl$_3$[53]	0.985	$R3m$	distorted	0.1368	8.6546	2.7202	160.45	3.43

[a]AZR = aziridinium, MHz = methylhydrazinium, MP = methylphosphonium, TMA = trimethylammonium, GA = Guanidinium.

62) space group.[37] CsPbI$_3$ crystallizes in the $Pm\bar{3}m$ space group above 583 K which can be quench cooled to a RT metastable perovskite phase in the $Pnam$ space group (no. 62).[33] The RT structures of CsPbX$_3$ (X = Cl, Br, I) and CsSnI$_3$ can be considered to be tilted perovskites with a Glazer notation of $a^+b^-b^-$ (Figure 3c). This tilting is induced by the smaller Cs$^+$ A-site cation leading to $\alpha < 0.9$; thus the structures approach the tilt limit. CsMI$_3$ (M = Sn, Pb) are unstable at RT and without stabilization will convert to a nonperovskite structure.[12,43] CsSnX$_3$ (X = Cl, Br) have $\alpha > 0.9$ which is larger than their Pb counterparts and as a result fit into the $Pm\bar{3}m$ nontilted space group.[46,64]

Germanium is smaller than Sn and Pb and has more pronounced lone pair (4s^2) effects. (A)GeI$_3$ (A = MA, FA)[52] and CsGeX$_3$ (X = Cl, Br, I)[52,65] crystallize in the polar $R3m$ space group (Figure 3d). The GeX$_6^{4-}$ octahedra are trigonally distorted with three elongated Ge−X bonds. With increasing A-site cation size in the CsGeI$_3$, MAGeI$_3$, and FAGeI$_3$ series, the Ge−I bonds elongate, resulting in a larger unit cell volume and higher D values (Table 1). The $R3m$ symmetry of Ge-based perovskites is caused by the small Ge with prominent lone pair effects and does not vary with A-site cation.[66] The same trends and symmetry occur true for (A)GeBr$_3$ (A = Cs$^+$, MA, FA) and (MA)GeCl$_3$.[54,67,68] All (A)GeX$_3$ compounds

have higher σ^2 and D values than their Pb and Sn counterparts (Table 1).

Notably, exotic cations larger than FA have been incorporated into the 3D halide perovskite structures. Methylhydrazinium (MHz) has been incorporated into (MHz)PbCl$_3$[42] and (MHz)PbBr$_3$[29] which both crystallize in the noncentrosymmetric $P2_1$ space group (Figure 3e).[69] Upon heating, these compounds undergo a phase change to structures with higher symmetry $Pm\bar{3}m$ (Br, 418 K) and $Pb2_1m$ (Cl, 342 K) space groups. The MHz cation highlights the unique effect of the A-site cation on the symmetry reduction due to not only the large size of the cation but also a contribution from coordination bonds of the terminal nitrogen groups in these large cations. In the RT crystal structure of (MHz)PbCl$_3$, the nitrogen coordinates selectively with specific lead sites leading to opposite distortions in every other layer and resulting in the low symmetry $P2_1$ space group at RT. Moreover, methylphosphonium (MP) and trimethylammonium (TMA) have been reported in distorted, Sn-based perovskite structures. (MP)SnBr$_3$ crystallizes in the Pc space group.[49] (TMA)SnBr$_3$ and (TMA)SnCl$_3$ crystallize in the $P2_1$ (Br) and $Cmc2_1$ (Cl) space groups (Figure 3f).[31,70] TMA has also been found in (TMA)GeCl$_3$ adopting the $Pnma$ or $Pna2_1$ space group at RT, though no crystal structure is available to
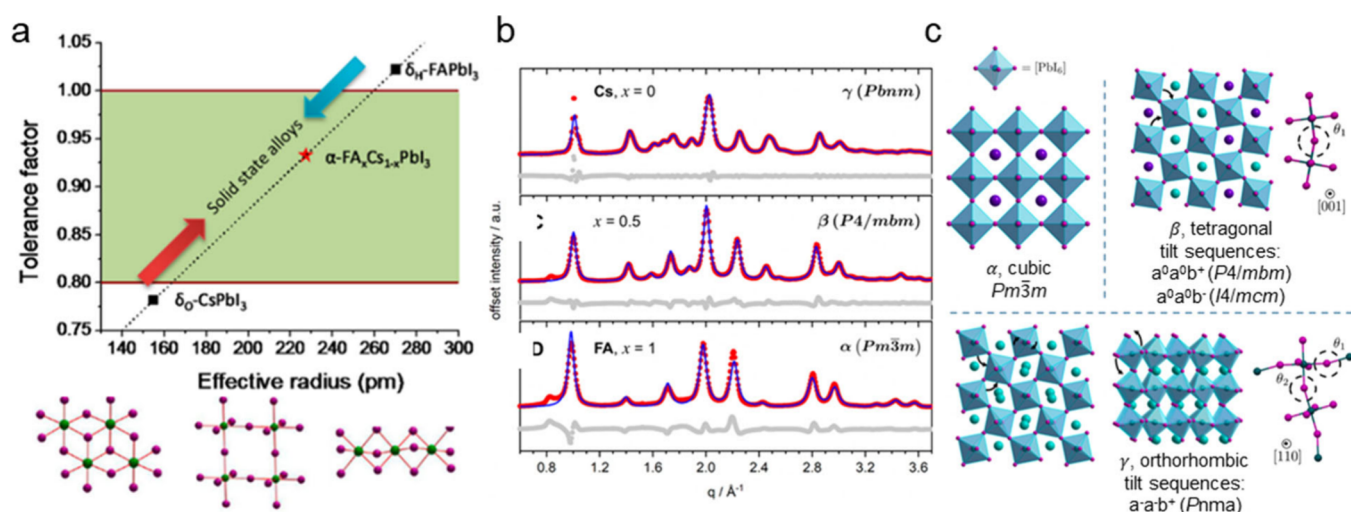
Figure 4. Stabilization of metastable perovskite phases via A-site cation alloying and large A-site cation 2D RP perovskites. (a) Tolerance factor versus effective A-site cation radius for solid-solutions of $(Cs_{1-x}FA_x)PbI_3$ with the corresponding crystal structures of the perovskite and nonperovskite phases below. (b) Rietveld refinement of pure $CsPbI_3$, mixed $(Cs_{0.5}FA_{0.5})PbI_3$, and $(FA)PbI_3$ nanocrystals with diffraction patterns. (c) Structures corresponding to panel b. Panel a is reproduced or adapted with permission from 102. Copyright 2016 American Chemical Society. Panels b and c are reproduced or adapted with permission from 103. Copyright 2020 American Chemical Society.

us.[71,72] Aziridinium (AZR) has been reported to be incorporated into $(AZR)PbX_3$ (X = Cl, Br, I) which crystallize in the $Pm\bar{3}m$ at RT.[36,73] It should be noted that the AZR cation is a highly reactive species due to the strain in a three-atom ring and undergoes rapid nucleophilic ring openings among other chemistries. While not explicitly studied to our knowledge, these AZR cations and their perovskites are likely prone to degradation via, for example, hydrolysis of AZR to the hydroxylammonium cation in the presence of water.

These low symmetry compounds are best described by the large distortions that such oversized A-site cations induce in the perovskite structure. All of these 3D halide perovskites incorporating large A-site cations have unusually large D and σ^2 due to the strain imposed on the M−X framework, which must contort to accommodate the oversized A-site cations. This distortion can be seen in Figure 3f, where the octahedron has extremely elongated bonds, which are at the edge of what is considered octahedral coordination. It is also worth noting the specific symmetry element of a 2_1 screw axis introduced in $(MHz)PbX_3$ (X = Cl, Br) and $(TMA)SnBr_3$ has become of interest for its helical nature.[74]

Briefly, there have been select demonstrations of fluoride based halide perovskites, specifically $CsPbF_3$[75] demonstrated experimentally and others explored computationally.[76−78] Other reports on related $CsMF_3$ structures are nonperovskite phases.[79] These compounds are an underexplored area of halide perovskite research and may not be promising as semiconductors, though creative research using alkaline metals as the metal site in the fluoride perovskite may lead to large ionic conductivities as have been observed previously.[80]

It should also be noted that we have focused on the room temperature phases of these 3D halide perovskites. Yet, there is extensive work on the temperature induced phase changes of halide perovskites. Usually the crystal symmetry is reduced as a halide perovskite is cooled (either from elevated temperatures or room temperature), which undergoes phase changes from the highest symmetry $Pm\bar{3}m$ to lower symmetry phases as outlined by a recent review.[81]

Exotic and Perovskite-like Structures. In addition to the typical AMX_3 perovskite structures, there has been an interest in identifying structures related to this motif for enhanced functionality or tailoring of the properties. One particular class is the $A_2MM'X_6$ (M = monovalent metal, M′ = trivalent metal) double perovskites (sometimes referred to as elpasolite based on the mineral K_2NaAlF_6).[82] These double perovskites can be broken into two classes: single metal multivalent and mixed-metal multivalent double perovskites. Some examples of single metal systems include $Cs_2Tl^{1+}Tl^{3+}Cl_6$[83] and $Cs_2Au^{1+}Au^{3+}Cl_6$.[84] A contemporary example of a mixed metal double perovskite is $Cs_2AgBiBr_6$ that grows in the $Fm\bar{3}m$ space group[85] and other examples recently reported.[86−88] These double perovskites have ordering due to the ionic size difference between Ag and Bi sites (sometimes deemed as "ordered double perovskites"). In these double perovskites, alkali metals are routinely utilized as an A-site cation. However, recent work has gone into making hybrid organic inorganic double perovskites using MA cations.[89] A more comprehensive discussion of double perovskites can be found here.[82]

Other unique perovskite-like structure types include the so-called "hollow" perovskites which incorporate a large divalent ethylenediammonium (en) cation.[90] In these structures, the divalent en cation not only occupies the A-site cation position but also induces metal and halide vacancies forming structures with the formula $(A)_{1-x}(en)_x(M)_{1-0.7x}(X)_{3-0.4x}$.[91−93] Because the M−X−M connectivity is not always completely corner-sharing in these structures, they are considered "perovskitoids" or perovskite-like; therefore, it could be debated if the associated organic cations should be called "A-site cations" in the strictest sense. One can consider these examples as at the boundary of the A-site cation chemistry in metal halide perovskites. Another interesting example is the incorporation of zwitterionic cystamine, with a formal negative charge on the sulfide and a positive charge on the amine. This forms a unique $(NH_3(CH_2)_2S)PbX_2$ (X = Cl, Br) perovskite structure, where the sulfur anion occupies the site of one halide as determined by X-ray pair distribution function analysis.[93]
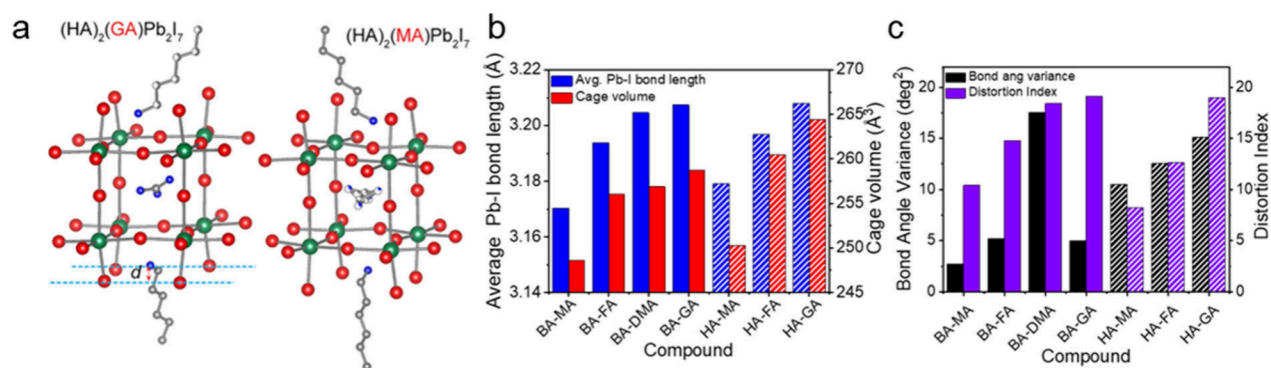
Figure 5. (a) Crystal structure of $(HA)_2(GA)PbI_7$ compared to that of $(HA)_2(MA)PbI_7$. (b) Average Pb−I bond length and cage volume of select large A-site cation RP perovskites showing an increase in length/size of inorganic framework with cation size. (c) Bond angle variance and distortion of RP perovskites showing the increase in distortion index with A-site cation size. BA = butylammonium, HA = hexylammonium, DMA = dimethylammonium, and GA = guanidinium. Panel a is reproduced or adapted with permission from 114. Copyright 2019 American Chemical Society. Panels b and c are reproduced or adapted with permission from 124. Copyright 2020 American Chemical Society.

A-Site Cation Orientation and Motion. FA and MA cations are highly disordered in the A-site cavity of AMX_3 at RT. Solid-state NMR can effectively capture this dynamic cation position and show that the MA cation in $(MA)PbX_3$ has no fixed position within the A-site cavity.[94,95] Instead, the NH_3^+ group reorients inside the cavity, interacting with the different halides in the lattice through hydrogen bonding, while the CH_3 group does not interact with the lattice. These are isotropic reorientations with activation energies on the order of 6−12 kJ/mol.[96] The activation energy of the reorientation decreases in the order of halide (Cl > Br > I), which can be attributed to the strength of the $NH_3 \cdots X$ hydrogen bonding. Based on 2D vibrational spectroscopy combined with ab initio molecular dynamics simulations, there are likely two reorientations occurring: a fast, local wobbling-in-a-cone motion (Figure 3g) and a slower 90° jump (Figure 3h).[32,95] The fast wobbling occurs on the 0.2−0.4 ps time scale, while the jump reorientation is 3 ps. Other reports based on neutron scattering suggest time scales are up to 14 ps.[97] The discrepancy is described in list of reorientation times presented by Gallop et al.[32] The FA cation behaves similarly, exhibiting rapid wobbling within a cone along with reorientation jumps.[98] The rotation about the N−N axis of FA has an energy barrier of 21 meV and occurs on the 8 ps time scale.[99] For further discussion on the cation dynamics in halide perovskites, we refer readers to recent reviews.[63,100] The cation reorientation at rapid time scales is important for the (high symmetry) space groups assigned above as the disordered MA and FA cations modeled in the crystallographic structures are likely the most accurate assignments reflective of the average (i.e., rotating) A-site cation. Another interesting observation shown through neutron inelastic spectroscopy and modeling is that the cations can have local ordering akin to ferroelectric domains that is coupled to dynamic octahedral tilts, suggesting the molecular rotations are coupled to the inorganic lattice instead of completely free rotations.[101]

A-Site Cation Alloying. Select 3D halide perovskite phases such as $(A)PbI_3$ (A= Cs^+, FA) are unstable as the perovskite phase at RT. However, these perovskites are very attractive for PV applications and can be stabilized via A-site cation alloying, among other techniques. An early example of alloying for stabilization was shown in $(Cs_{1-x}FA_x)PbI_3$ thin films.[102] By alloying Cs−FA, the tolerance factor was effectively tuned between the small Cs and large FA structures

(Figure 4a) and resulted in stable halide perovskite materials. Grazing incidence wide-angle X-ray scattering on nanocrystal films further revealed that tuning the FA/Cs ratio in $(Cs_{1-x}FA_x)PbI_3$ changed the tilting and symmetry of the crystal structure (Figure 4b).[103,104] At low Cs content (x > 0.7), the high symmetry $Pm\bar{3}m$ structure is favored (Figure 4c). By incorporation of more FA (0.7 > x > 0.2), a lower symmetry $P4/mbm$ structure is formed, analogous to what is observed in $(MA)PbI_3$ ($I4/mcm$). At high Cs concentrations (x > 0.2), the structure adopts the tilted $Pbnm$ space group. Other examples of A-site cation alloying at room temperature do not show changes in symmetry or tilting, but simple expansion/contraction of the unit cell based on the cation size.[37,105−108] It should also be noted that there is evidence of A-site cation mobility in these alloyed structures under external stimuli, such as an electrical bias. While A-site cations are not as mobile as halide anions,[104,109] over the time scale of device operation and under the external stimuli of light soaking and bias the A-site cations do begin to phase segregate.[110] A-site cation alloying and more generally compositional engineering including the metal and halide ions has proven to be a key component of making high efficiency perovskite solar cells, including tandem perovskite solar cells, and is described in detail in many recent reviews focused on perovskite solar cells.[19,111−113]

A-Site Cations in 2D RP Perovskites. 2D $(A')_2(A)_{n-1}M_nX_{3n+1}$ Ruddlesden−Popper (RP) perovskites can accommodate a larger range of A-site cations than AMX_3 halide perovskites.[114−117] In RP perovskites, the layers of the inorganic M−X framework are interceded by flexible long chain ammonium spacer cations (A'),[17] which stabilizes the perovskite cages of n > 1 RP perovskites that incorporate large A-site cations into the 12-coordinate A-site pocket. The large guanidinium (GA) cation has been incorporated into $(A')_2$ (GA)Pb_2I_7 with A' = n-butylammonium (BA),[116] n-pentylammonium (PA),[118,119] and n-hexylammonium (HA)[114] and confirmed by single-crystal X-ray crystallography. The GA cation alone (i.e., if attempted to grow as an AMX_3 perovskite) forms a nonperovskite structure lacking the 12-coordinate A-site cavity.[114] In these RP structures with a large A-site cation, the volume of the A-site cavity is dramatically increased relative to the corresponding $(A')(MA)Pb_2I_7$ (Figure 5a). In $(HA)_2(A)Pb_2I_7$ with A = MA and GA structure, there is a clear increase in Pb−I bond length and A-site cavity volume

when the larger GA cation is incorporated, which matches the trend for other A′ cations such as PA.[118] Furthermore, the large GA cation distorts the PbI_6^{4-} octahedra, resulting in larger σ^2 and D relative to $(A')(MA)Pb_2I_7$ structures (Figure 5b,c). Similarly, other $n = 2$ RP perovskite compounds with larger cations, such as $(A')(FA)Pb_2I_7$ (A′ = BA,[116] HA[120]) and $(A')_2(DMA)Pb_2I_7$ (A′ = BA,[116] PA[121]), exhibit elongated Pb−I bonds and larger distortion relative to RP perovskites with MA cations, though to a lesser extent than GA (Figure 5b,c). Comprehensive structural analysis comparing across a series of six A-cations (MA, FA, DMA, EA, GA, and AA) in $(PA)_2(A)Pb_2I_7$ demonstrated the significance of the shape, polarity, and hydrogen bonding interactions of the A-cations, beyond simply cation size, in dictating the local distortions and expansion of the perovskite cage which has consequences on the structural symmetry.[122] Similar to the 3D perovskites, enhanced ns^2 lone pair expression in germanium and tin $(A')_2(A)X_2I_7$ RP perovskites can lead to more significant octahedral distortions across the A-cation[66] that are the most pronounced for germanium analogues,[123] but are further dependent on the choice of A′.

Higher n-value RP perovskite structures with large A-site cations follow the same trend: the Pb−I bonds in $(A')_2(EA)_2Pb_3I_{10}$ (EA = ethylammonium, A′ = BA,[124,125] PA,[126] HA[127]) are elongated and induce a larger A-site cavity compared to $(BA)_2(MA)_2Pb_3I_{10}$. Moreover, the changes in Pb−I bonding in these $n = 3$ RP perovskite structures depend on whether the octahedra is in the inner layer or the two outer layers of PbI_6^{4-} octahedra. The inner layer has significantly more distorted octahedra, as it is templated by two EA cations on both sides with large steric interactions. Whereas the outer layers are templated by one EA cation and a more flexible BA cation, leading to less distorted octahedra. Similar to the iodides, the smaller bromide based RP structures also feature increasing D, σ^2, bond lengths, and cage volume as the A-site cation size increases. $(BA)_2(A)Pb_2Br_7$ (A= Cs,[128,129] MA,[130] FA[131]) form in the $Cmc2_1$ space group at RT. Moving to the larger EA cation, multiple $(A')(EA)_{n-1}Pb_nBr_{3n+1}$ structures have been demonstrated with the A′ spacer cation varying from EA,[132] BA,[133] isobutylammonium (IBA),[134] and 4-aminomethyl-1-cyclohexanecarboxylate.[135] The structure $(EA)_4Pb_3X_{10}$ (X = Cl, Br) form a unique RP layered structure where the EA cation serves as both the A-site cation as well as the spacer cation.[132,136] A unique, a cyclic A-site cation 1,2,4-triazolium (Tz) has been incorporated into $(IPA)_2(Tz)_{n-1}Pb_nBr_{3n+1}$ ($n = 2$, 3) with large distortions in the octahedra.[137] Other large cations such as DMA and MHz have also been introduced to the bromide RP halide perovskites.[138] In addition, 2D Dion−Jacobson phase with divalent spacer cations (A′) interceding the layers has also had large A-site cations incorporated.[139−141] In general, incorporation of large A-site cations into the RP halide perovskites promotes structural changes similar to those of the AMX_3 halide perovskites with larger A-site cation, where the octahedra stretch and distort to accommodate the size of the cation. The ability to incorporate even larger cations in the 2D RP halides compared to 3D perovskites is a result of the compressive strain accommodated by the spacer cation being flexible.[114,116]

Influence of A-Site Cation on Optical Properties. A recent review on the growth of single crystal halide perovskites shows the bandgap energy (E_g) slightly varies with the growth conditions of the compound, yet general trends can be

discussed as they relate the crystal structure to optical properties.[142] The series Cl > Br > I and Ge > Pb > Sn and are ordered from largest to smallest bandgap energy (E_g).[12,52,143] The A-site cation does not significantly contribute to the density of states making up the conduction and valence band but indirectly affects the band gap and optoelectronic properties by templating the bonding of the M−X framework. Tilted structures such as $CsPbI_3$ have a larger E_g (1.72 eV) relative to the nontilted structure $(FA)PbI_3$ (1.41 eV).[144,145] This effect is the result of a shift in the overlap of the M and X orbitals due to the tilting.[146,147] Based on DFT calculations, changes in symmetry do not significantly alter the band dispersion, only the band gap.[148]

The E_g of alloyed $(Cs_{1-x}Rb_x)PbX_3$ (X = Cl, Br) and $(FA_{1-x}MA_x)PbI_3$ decrease linearly as the tolerance factor increases (i.e., the average A-site cation size gets larger).[37,149] Focusing the trendlines on a single metal and halide (constant r_M and r_X) and comparing the E_g of $APbX_3$ (X = Cl, Br, I) versus the tolerance factor, we can observe a bowing trend with increasing A-site cation size (Figure 6a). In the $APbCl_3$ series, the tilted $CsPbCl_3$ has a wider gap than the less tilted $(MA)PbCl_3$ which displays the narrowest E_g. The larger stretch limit $(FA)PbCl_3$ structure has a higher E_g due to the decreased M−X overlap as a result of the elongated Pb−Cl bonds. The even larger $(MHz)PbCl_3$ has the largest E_g, due to even more elongated bonds and distortion in the octahedra. This trend seems consistent with the $APbBr_3$ and $APbI_3$ series, though there are fewer data points to compare. Plotting the band gap versus tolerance factor of AMI_3 (constant r_I) for different M (Pb, Sn, Ge) and A-site cations reveals a similar trend (Figure 6b). The perovskite structures with a moderate tolerance factor (0.9−1.0, the wide band in the middle) have the smallest E_g, and the E_g increases below and above this range. For $\alpha < 0.9$ (small A-site cation for the structure), tilting will raise the E_g. At $\alpha > 1$ (A-site cation too big for the structure), the M−X bonds are elongated causing an increase in E_g. In moderate range ($0.9 < \alpha < 1.0$) the curve is flat. This trend is consistent with the observations in RP perovskites which have an expanded range of A-site cation sizes. Figure 6c shows nanocrystals of RP perovskites $(HA)_2(A)Pb_2I_7$ (HA = hexylammonium) with various A-site cations ranging from small Cs to large guanidinium (GA) and acetamidinium (AA) cations. There is a parabolic trend between the bandgap and cation size similar to the trends with 3D perovskite and tolerance factor, but showing more definitively the effect of the Pb−I stretching (induced by large A-cations) increasing the band gap. An interesting observation is that by external pressure applied, which effectively shortens Pb−I bond distance, the band gap begins to decrease.[150,151] This shows that elongation of the bond distances increases the band gap, while compression decreases the band gap, effectively getting both ends of the spectrum. A more comprehensive review of halide perovskites under pressure can be found here.[152]

CONCLUSIONS

Metal halide perovskites are in the process of being commercialized as solar absorbers and are promising materials for other optoelectronic applications owing in part to their structural tunability. As a comparatively less studied and discussed compositional tuning approach, the A-site cation provides an alternative way to tune the perovskite crystal structures and bonding and thus influences the physical properties of the materials. In this review, we have provided a
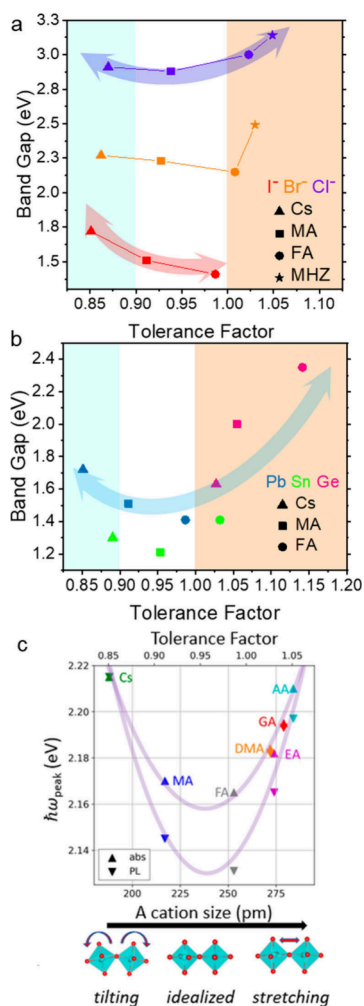
Figure 6. Relationship of band gap to Goldsmidt tolerance factor in various 3D AMX_3 perovskites. (a) Band gap versus tolerance factor of $APbX_3$ showing the band gap decrease with larger tolerance factor for each halide series until reaching a stretching limit ($\sim\alpha > 1$), where the band gap increases. (b) Band gap vs tolerance factor for AMI_3 with a similar downward sloping trend for $\sim\alpha < 0.9$, followed by increasing band gap at $\sim\alpha > 1$ (shaded for clarity). (c) Relationship of A-site cation size and absorbance/photoluminescence in nanocrystals of large A-site cation $n = 2$ RP perovskites. Panel c is reproduced or adapted with permission from 115. Copyright 2020 American Chemical Society.

further tuning the A-site cations in halide perovskites.[153] This includes enhancing nonlinear (second harmonic generation, ferroelectricity, etc.) properties and Rashba band splitting,[59,122,123] which are dependent on the symmetry of the material, in particular materials with noncentrosymmetric polar space groups.[154,155] In addition, many phenomena exhibited by halide perovskite materials could be potentially useful for computational information science, including superfluorescence,[156] control over spin polarization,[7] and single photon emitters.[157] While not explicitly dependent on structural symmetry, these properties can be enhanced or modulated by utilizing new compositions enabled by A-site cation chemistry. Third, it appears there has been a significant amount of research into the narrow band gap lead and tin iodide based perovskites owing to their utility in solar cells. However, since many of these potential applications beyond solar cells do not require a narrow band gap (as is the case for solar), it is worthwhile for researchers to further explore the chloride and bromide based perovskites, which often exhibit more diverse and unique structures enabled by large A-site cations (such as the interesting $P2_1$ (TMA)SnBr$_3$ structures[70]). At the core of these potential applications, exploring new halide perovskite structures enabled by A-site cations, developing new 2D RP perovskite structures with expanded A-site cations, and the resulting enhanced structural control in halide perovskites will aid in future endeavors of halide perovskite materials research for broad applications.

■ AUTHOR INFORMATION

Corresponding Author

Matthew P. Hautzinger − *National Renewable Energy Laboratory, Golden, Colorado 80401, United States;* ⓘ orcid.org/0000-0002-4764-3076; Email: matthew.hautzinger@nrel.gov

Authors

Willa Mihalyi-Koch − *Department of Chemistry, University of Wisconsin-Madison, Madison, Wisconsin 53706, United States;* ⓘ orcid.org/0000-0003-2984-7611
Song Jin − *Department of Chemistry, University of Wisconsin-Madison, Madison, Wisconsin 53706, United States;* ⓘ orcid.org/0000-0001-8693-7010

Complete contact information is available at:
https://pubs.acs.org/10.1021/acs.chemmater.4c02043

Notes

■ ACKNOWLEDGMENTS

comprehensive summary of 3D AMX_3 halide perovskite structures with a diverse set of A-site cations with a focus on empirical results demonstrating the influence of the A-site cation on the structural distortion and overall perovskite structure. Further discussion on A-site cation motion, alloying, and expanded A-site cation compositions in 2D RP perovskites is provided to further explain the impact of the A-site cations. The crystal structure is then correlated with band gap to understand the relationship of the halide perovskite structure on optical properties. Using A-site cations together with other compositional changes to access refined structure and property tuning could drive continued progress in the chemistry, properties, and applications of halide perovskites and broader metal halide materials.

In addition to enhancing photophysical properties for improved optoelectronic devices already demonstrated by current literature, many areas of research can be aided by

■ REFERENCES

(1) Kojima, A.; Teshima, K.; Shirai, Y.; Miyasaka, T. Organometal Halide Perovskites as Visible-Light Sensitizers for Photovoltaic Cells. *J. Am. Chem. Soc.* **2009**, *131* (17), 6050−6051.

(2) Lee, M. M.; Teuscher, J.; Miyasaka, T.; Murakami, T. N.; Snaith, H. J. Efficient Hybrid Solar Cells Based on Meso-Superstructured Organometal Halide Perovskites. *Science* **2012**, *338* (6107), 643−647.

(3) Quan, L. N.; Rand, B. P.; Friend, R. H.; Mhaisalkar, S. G.; Lee, T.-W.; Sargent, E. H. Perovskites for Next-Generation Optical Sources. *Chem. Rev.* **2019**, *119* (12), 7444−7477.

(4) Zhu, H.; Fu, Y.; Meng, F.; Wu, X.; Gong, Z.; Ding, Q.; Gustafsson, M. V.; Trinh, M. T.; Jin, S.; Zhu, X.-Y. Lead Halide Perovskite Nanowire Lasers with Low Lasing Thresholds and High Quality Factors. *Nat. Mater.* **2015**, *14* (6), 636−642.

(5) Zhou, Y.; Chen, J.; Bakr, O. M.; Mohammed, O. F. Metal Halide Perovskites for X-Ray Imaging Scintillators and Detectors. *ACS Energy Lett.* **2021**, *6* (2), 739−768.

(6) Chin, X. Y.; Cortecchia, D.; Yin, J.; Bruno, A.; Soci, C. Lead Iodide Perovskite Light-Emitting Field-Effect Transistor. *Nat. Commun.* **2015**, *6* (1), 7383.

(7) Lu, H.; Vardeny, Z. V.; Beard, M. C. Control of Light, Spin and Charge with Chiral Metal Halide Semiconductors. *Nat. Rev. Chem.* **2022**, *6* (7), 470−485.

(8) Hautzinger, M. P.; Pan, X.; Hayden, S. C.; Ye, J. Y.; Jiang, Q.; Wilson, M. J.; Phillips, A. J.; Dong, Y.; Raulerson, E. K.; Leahy, I. A.; Jiang, C.-S.; Blackburn, J. L.; Luther, J. M.; Lu, Y.; Jungjohann, K.; Vardeny, Z. V.; Berry, J. J.; Alberi, K.; Beard, M. C. Room-Temperature Spin Injection across a Chiral Perovskite/III−V Interface. *Nature* **2024**, *631*, 307.

(9) Dunlap-Shohl, W. A.; Zhou, Y.; Padture, N. P.; Mitzi, D. B. Synthetic Approaches for Halide Perovskite Thin Films. *Chem. Rev.* **2019**, *119* (5), 3193−3295.

(10) Dey, A.; Ye, J.; De, A.; Debroye, E.; Ha, S. K.; Bladt, E.; Kshirsagar, A. S.; Wang, Z.; Yin, J.; Wang, Y.; Quan, L. N.; Yan, F.; Gao, M.; Li, X.; Shamsi, J.; Debnath, T.; Cao, M.; Scheel, M. A.; Kumar, S.; Steele, J. A.; Gerhard, M.; Chouhan, L.; Xu, K.; Wu, X.; Li, Y.; Zhang, Y.; Dutta, A.; Han, C.; Vincon, I.; Rogach, A. L.; Nag, A.; Samanta, A.; Korgel, B. A.; Shih, C.-J.; Gamelin, D. R.; Son, D. H.; Zeng, H.; Zhong, H.; Sun, H.; Demir, H. V.; Scheblykin, I. G.; Mora-Seró, I.; Stolarczyk, J. K.; Zhang, J. Z.; Feldmann, J.; Hofkens, J.; Luther, J. M.; Pérez-Prieto, J.; Li, L.; Manna, L.; Bodnarchuk, M. I.; Kovalenko, M. V.; Roeffaers, M. B. J.; Pradhan, N.; Mohammed, O. F.; Bakr, O. M.; Yang, P.; Müller-Buschbaum, P.; Kamat, P. V.; Bao, Q.; Zhang, Q.; Krahne, R.; Galian, R. E.; Stranks, S. D.; Bals, S.; Biju, V.; Tisdale, W. A.; Yan, Y.; Hoye, R. L. Z.; Polavarapu, L. State of the Art and Prospects for Halide Perovskite Nanocrystals. *ACS Nano* **2021**, *15* (7), 10775−10981.

(11) Fu, Y.; Zhu, H.; Chen, J.; Hautzinger, M. P.; Zhu, X.-Y.; Jin, S. Metal Halide Perovskite Nanostructures for Optoelectronic Applications and the Study of Physical Properties. *Nat. Rev. Mater.* **2019**, *4* (3), 169−188.

(12) Stoumpos, C. C.; Malliakas, C. D.; Kanatzidis, M. G. Semiconducting Tin and Lead Iodide Perovskites with Organic Cations: Phase Transitions, High Mobilities, and Near-Infrared Photoluminescent Properties. *Inorg. Chem.* **2013**, *52* (15), 9019−9038.

(13) Stoumpos, C. C.; Cao, D. H.; Clark, D. J.; Young, J.; Rondinelli, J. M.; Jang, J. I.; Hupp, J. T.; Kanatzidis, M. G. Ruddlesden−Popper Hybrid Lead Iodide Perovskite 2D Homologous Semiconductors. *Chem. Mater.* **2016**, *28* (8), 2852−2867.

(14) Ruddlesden, S. N.; Popper, P. The Compound Sr\sb 3Ti\sb 2O\sb 7 and Its Structure. *Acta Crystallogr.* **1958**, *11* (1), 54−55.

(15) Mao, L.; Ke, W.; Pedesseau, L.; Wu, Y.; Katan, C.; Even, J.; Wasielewski, M. R.; Stoumpos, C. C.; Kanatzidis, M. G. Hybrid Dion−Jacobson 2D Lead Iodide Perovskites. *J. Am. Chem. Soc.* **2018**, *140* (10), 3775−3783.

(16) Saparov, B.; Mitzi, D. B. Organic−Inorganic Perovskites: Structural Versatility for Functional Materials Design. *Chem. Rev.* **2016**, *116* (7), 4558−4596.

(17) Li, X.; Hoffman, J. M.; Kanatzidis, M. G. The 2D Halide Perovskite Rulebook: How the Spacer Influences Everything from the Structure to Optoelectronic Device Efficiency. *Chem. Rev.* **2021**, *121* (4), 2230−2291.

(18) Leung, T. L.; Ahmad, I.; Syed, A. A.; Ng, A. M. C.; Popović, J.; Djurišić, A. B. Stability of 2D and Quasi-2D Perovskite Materials and Devices. *Commun. Mater.* **2022**, *3* (1), 63.

(19) Lee, J.-W.; Tan, S.; Seok, S. I.; Yang, Y.; Park, N.-G. Rethinking the A Cation in Halide Perovskites. *Science* **2022**, *375* (6583), No. eabj1186.

(20) Goldschmidt, V. M. Die Gesetze Der Krystallochemie. *Naturwissenschaften* **1926**, *14* (21), 477−485.

(21) Kieslich, G.; Sun, S.; Cheetham, A. K. Solid-State Principles Applied to Organic−Inorganic Perovskites: New Tricks for an Old Dog. *Chem. Sci.* **2014**, *5* (12), 4712−4715.

(22) Filip, M. R.; Giustino, F. The Geometric Blueprint of Perovskites. *Proc. Natl. Acad. Sci. U. S. A.* **2018**, *115* (21), 5397−5402.

(23) Travis, W.; Glover, E. N. K.; Bronstein, H.; Scanlon, D. O.; Palgrave, R. G. On the Application of the Tolerance Factor to Inorganic and Hybrid Halide Perovskites: A Revised System. *Chem. Sci.* **2016**, *7* (7), 4548−4556.

(24) Bartel, C. J.; Sutton, C.; Goldsmith, B. R.; Ouyang, R.; Musgrave, C. B.; Ghiringhelli, L. M.; Scheffler, M. New Tolerance Factor to Predict the Stability of Perovskite Oxides and Halides. *Sci. Adv.* **2019**, *5* (2), No. eaav0693.

(25) Glazer, A. M. The Classification of Tilted Octahedra in Perovskites. *Acta Crystallogr. Sect. B* **1972**, *28* (11), 3384−3392.

(26) Howard, C. J.; Stokes, H. T. Structures and Phase Transitions in Perovskites − a Group-Theoretical Approach. *Acta Crystallogr., Sect. A* **2005**, *61* (1), 93−111.

(27) Baur, W. H. The Geometry of Polyhedral Distortions. Predictive Relationships for the Phosphate Group. *Acta Crystallogr. Sect. B* **1974**, *30* (5), 1195−1215.

(28) Robinson, K.; Gibbs, G. V.; Ribbe, P. H. Quadratic Elongation: A Quantitative Measure of Distortion in Coordination Polyhedra. *Science* **1971**, *172* (3983), 567−570.

(29) Mączka, M.; Ptak, M.; Gągor, A.; Stefańska, D.; Zaręba, J. K.; Sieradzki, A. Methylhydrazinium Lead Bromide: Noncentrosymmetric Three-Dimensional Perovskite with Exceptionally Large Framework Distortion and Green Photoluminescence. *Chem. Mater.* **2020**, *32* (4), 1667−1673.

(30) Thiele, G.; Serr, B. R. Crystal Structure of Trimethylammonium Tribromostannate(II), (CH3)3NHSnBr3. *Z. Kristallogr.* **1996**, *211* (1), 46−46.

(31) Dang, Y.; Zhong, C.; Zhang, G.; Ju, D.; Wang, L.; Xia, S.; Xia, H.; Tao, X. Crystallographic Investigations into Properties of Acentric Hybrid Perovskite Single Crystals NH(CH3)3SnX3 (X = Cl, Br). *Chem. Mater.* **2016**, *28* (19), 6968−6974.

(32) Gallop, N. P.; Selig, O.; Giubertoni, G.; Bakker, H. J.; Rezus, Y. L. A.; Frost, J. M.; Jansen, T. L. C.; Lovrincic, R.; Bakulin, A. A. Rotational Cation Dynamics in Metal Halide Perovskites: Effect on Phonons and Material Properties. *J. Phys. Chem. Lett.* **2018**, *9* (20), 5987−5997.

(33) Sutton, R. J.; Filip, M. R.; Haghighirad, A. A.; Sakai, N.; Wenger, B.; Giustino, F.; Snaith, H. J. Cubic or Orthorhombic? Revealing the Crystal Structure of Metastable Black-Phase CsPbI3 by Theory and Experiment. *ACS Energy Lett.* **2018**, *3* (8), 1787−1794.

(34) Szafrański, M.; Katrusiak, A. Mechanism of Pressure-Induced Phase Transitions, Amorphization, and Absorption-Edge Shift in

Photovoltaic Methylammonium Lead Iodide. *J. Phys. Chem. Lett.* **2016**, *7* (17), 3458−3466.

(35) Zhumekenov, A. A.; Saidaminov, M. I.; Haque, M. A.; Alarousu, E.; Sarmah, S. P.; Murali, B.; Dursun, I.; Miao, X.-H.; Abdelhady, A. L.; Wu, T.; Mohammed, O. F.; Bakr, O. M. Formamidinium Lead Halide Perovskite Crystals with Unprecedented Long Carrier Dynamics and Diffusion Length. *ACS Energy Lett.* **2016**, *1* (1), 32−37.

(36) Petrosova, H. R.; Kucheriv, O. I.; Shova, S.; Gural'skiy, I. A. Aziridinium Cation Templating 3D Lead Halide Hybrid Perovskites. *Chem. Commun.* **2022**, *58* (38), 5745−5748.

(37) Linaburg, M. R.; McClure, E. T.; Majher, J. D.; Woodward, P. M. Cs1−xRbxPbCl3 and Cs1−xRbxPbBr3 Solid Solutions: Understanding Octahedral Tilting in Lead Halide Perovskites. *Chem. Mater.* **2017**, *29* (8), 3507−3514.

(38) Jaffe, A.; Lin, Y.; Beavers, C. M.; Voss, J.; Mao, W. L.; Karunadasa, H. I. High-Pressure Single-Crystal Structures of 3D Lead-Halide Hybrid Perovskites and Pressure Effects on Their Electronic and Optical Properties. *ACS Cent. Sci.* **2016**, *2* (4), 201−209.

(39) Hanusch, F. C.; Wiesenmayer, E.; Mankel, E.; Binek, A.; Angloher, P.; Fraunhofer, C.; Giesbrecht, N.; Feckl, J. M.; Jaegermann, W.; Johrendt, D.; Bein, T.; Docampo, P. Efficient Planar Heterojunction Perovskite Solar Cells Based on Formamidinium Lead Bromide. *J. Phys. Chem. Lett.* **2014**, *5* (16), 2791−2795.

(40) Nandi, P.; Giri, C.; Swain, D.; Manju, U.; Topwal, D. Room Temperature Growth of CH3NH3PbCl3 Single Crystals by Solvent Evaporation Method. *CrystEngComm* **2019**, *21* (4), 656−661.

(41) Govinda, S.; Kore, B. P.; Swain, D.; Hossain, A.; De, C.; Guru Row, T. N.; Sarma, D. D. Critical Comparison of FAPbX3 and MAPbX3 (X = Br and Cl): How Do They Differ? *J. Phys. Chem. C* **2018**, *122* (25), 13758−13766.

(42) Mączka, M.; Gagor, A.; Zaręba, J. K.; Stefanska, D.; Drozd, M.; Balciunas, S.; Šimėnas, M.; Banys, J.; Sieradzki, A. Three-Dimensional Perovskite Methylhydrazinium Lead Chloride with Two Polar Phases and Unusual Second-Harmonic Generation Bistability above Room Temperature. *Chem. Mater.* **2020**, *32* (9), 4072−4082.

(43) Yamada, K.; Funabiki, S.; Horimoto, H.; Matsui, T.; Okuda, T.; Ichiba, S. Structural Phase Transitions of the Polymorphs of CsSnI3 by Means of Rietveld Analysis of the X-Ray Diffraction. *Chem. Lett.* **1991**, *20* (5), 801−804.

(44) Takahashi, Y.; Obara, R.; Lin, Z.-Z.; Takahashi, Y.; Naito, T.; Inabe, T.; Ishibashi, S.; Terakura, K. Charge-Transport in Tin-Iodide Perovskite CH3NH3SnI3: Origin of High Conductivity. *Dalton Trans.* **2011**, *40* (20), 5563−5568.

(45) Schueller, E. C.; Laurita, G.; Fabini, D. H.; Stoumpos, C. C.; Kanatzidis, M. G.; Seshadri, R. Crystal Structure Evolution and Notable Thermal Expansion in Hybrid Perovskites Formamidinium Tin Iodide and Formamidinium Lead Bromide. *Inorg. Chem.* **2018**, *57* (2), 695−701.

(46) Fabini, D. H.; Laurita, G.; Bechtel, J. S.; Stoumpos, C. C.; Evans, H. A.; Kontos, A. G.; Raptis, Y. S.; Falaras, P.; Van der Ven, A.; Kanatzidis, M. G.; Seshadri, R. Dynamic Stereochemical Activity of the Sn2+ Lone Pair in Perovskite CsSnBr3. *J. Am. Chem. Soc.* **2016**, *138* (36), 11820−11832.

(47) Li, B.; Long, R.; Xia, Y.; Mi, Q. All-Inorganic Perovskite CsSnBr3 as a Thermally Stable, Free-Carrier Semiconductor. *Angew. Chem., Int. Ed.* **2018**, *57* (40), 13154−13158.

(48) Tao, S.; Schmidt, I.; Brocks, G.; Jiang, J.; Tranca, I.; Meerholz, K.; Olthof, S. Absolute Energy Level Positions in Tin- and Lead-Based Halide Perovskites. *Nat. Commun.* **2019**, *10* (1), 2560.

(49) Zhang, H.-Y.; Chen, X.-G.; Zhang, Z.-X.; Song, X.-J.; Zhang, T.; Pan, Q.; Zhang, Y.; Xiong, R.-G. Methylphosphonium Tin Bromide: A 3D Perovskite Molecular Ferroelectric Semiconductor. *Adv. Mater.* **2020**, *32* (47), No. 2005213.

(50) Yamada, K.; Kuranaga, Y.; Ueda, K.; Goto, S.; Okuda, T.; Furukawa, Y. Phase Transition and Electric Conductivity of ASnCl3 (A = Cs and CH3NH3). *Bull. Chem. Soc. Jpn.* **1998**, *71* (1), 127−134.

(51) Szafrański, M.; Ståhl, K. Crystal Structure and Phase Transitions in Perovskite-like C(NH2)3SnCl3. *J. Solid State Chem.* **2007**, *180* (8), 2209−2215.

(52) Stoumpos, C. C.; Frazer, L.; Clark, D. J.; Kim, Y. S.; Rhim, S. H.; Freeman, A. J.; Ketterson, J. B.; Jang, J. I.; Kanatzidis, M. G. Hybrid Germanium Iodide Perovskite Semiconductors: Active Lone Pairs, Structural Distortions, Direct and Indirect Energy Gaps, and Strong Nonlinear Optical Properties. *J. Am. Chem. Soc.* **2015**, *137* (21), 6804−6819.

(53) Lin, Z.-G.; Tang, L.-C.; Chou, C.-P. Characterization and Properties of Infrared NLO Crystals: AGeX3 (A = Rb, Cs; X = Cl, Br). *J. Cryst. Growth* **2008**, *310* (13), 3224−3229.

(54) Liu, Y.; Gong, Y.-P.; Geng, S.; Feng, M.-L.; Manidaki, D.; Deng, Z.; Stoumpos, C. C.; Canepa, P.; Xiao, Z.; Zhang, W.-X.; Mao, L. Hybrid Germanium Bromide Perovskites with Tunable Second Harmonic Generation. *Angew. Chem., Int. Ed.* **2022**, *61* (43), No. e202208875.

(55) Knop, O.; Wasylishen, R. E.; White, M. A.; Cameron, T. S.; Oort, M. J. M. V. Alkylammonium Lead Halides. Part 2. CH3NH3PbX3 (X = Cl, Br, I) Perovskites: Cuboctahedral Halide Cages with Isotropic Cation Reorientation. *Can. J. Chem.* **1990**, *68* (3), 412−422.

(56) Saidaminov, M. I.; Abdelhady, A. L.; Murali, B.; Alarousu, E.; Burlakov, V. M.; Peng, W.; Dursun, I.; Wang, L.; He, Y.; Maculan, G.; Goriely, A.; Wu, T.; Mohammed, O. F.; Bakr, O. M. High-Quality Bulk Hybrid Perovskite Single Crystals within Minutes by Inverse Temperature Crystallization. *Nat. Commun.* **2015**, *6* (1), 7586.

(57) Frohna, K.; Deshpande, T.; Harter, J.; Peng, W.; Barker, B. A.; Neaton, J. B.; Louie, S. G.; Bakr, O. M.; Hsieh, D.; Bernardi, M. Inversion Symmetry and Bulk Rashba Effect in Methylammonium Lead Iodide Perovskite Single Crystals. *Nat. Commun.* **2018**, *9* (1), 1829.

(58) Kawamura, Y.; Mashiyama, H.; Hasebe, K. Structural Study on Cubic−Tetragonal Transition of CH3NH3PbI3. *J. Phys. Soc. Jpn.* **2002**, *71* (7), 1694−1697.

(59) Fu, Y.; Jin, S.; Zhu, X.-Y. Stereochemical Expression of Ns2 Electron Pairs in Metal Halide Perovskites. *Nat. Rev. Chem.* **2021**, *5*, 838.

(60) Kontos, A. G.; Manolis, G. K.; Kaltzoglou, A.; Palles, D.; Kamitsos, E. I.; Kanatzidis, M. G.; Falaras, P. Halogen−NH2+ Interaction, Temperature-Induced Phase Transition, and Ordering in (NH2CHNH2)PbX3 (X = Cl, Br, I) Hybrid Perovskites. *J. Phys. Chem. C* **2020**, *124* (16), 8479−8487.

(61) Weller, M. T.; Weber, O. J.; Frost, J. M.; Walsh, A. Cubic Perovskite Structure of Black Formamidinium Lead Iodide, α-[HC(NH2)2]PbI3, at 298 K. *J. Phys. Chem. Lett.* **2015**, *6* (16), 3209−3212.

(62) Fabini, D. H.; Stoumpos, C. C.; Laurita, G.; Kaltzoglou, A.; Kontos, A. G.; Falaras, P.; Kanatzidis, M. G.; Seshadri, R. Reentrant Structural and Optical Properties and Large Positive Thermal Expansion in Perovskite Formamidinium Lead Iodide. *Angew. Chem., Int. Ed.* **2016**, *55* (49), 15392−15396.

(63) Kubicki, D. J.; Stranks, S. D.; Grey, C. P.; Emsley, L. NMR Spectroscopy Probes Microstructure, Dynamics and Doping of Metal Halide Perovskites. *Nat. Rev. Chem.* **2021**, *5* (9), 624−645.

(64) Bulanova, G. G.; Podleskaya, A. V.; Soboleva, L. V.; Soklakov, A. I. Investigation into Tin-Cesium Chlorides CsSnCl3 and Cs2SnCl6. *Izv. Akad. Nauk SSSR Neorganicheskie Mater.* **1972**, *8* (11), 1930−1932.

(65) Thiele, G.; Rotter, H. W.; Schmidt, K. D. Kristallstrukturen Und Phasentransformationen von Caesiumtrihalogenogermanaten(II) CsGeX3 (X = Cl, Br, I). *Z. Für Anorg. Allg. Chem.* **1987**, *545* (2), 148−156.

(66) Li, X.; Guan, Y.; Li, X.; Fu, Y. Stereochemically Active Lone Pairs and Nonlinear Optical Properties of Two-Dimensional Multilayered Tin and Germanium Iodide Perovskites. *J. Am. Chem. Soc.* **2022**, *144* (39), 18030−18042.

(67) Yamada, K.; Mikawa, K.; Okuda, T.; Knight, K. S. Static and Dynamic Structures of CD3ND3GeCl3 Studied by TOF High

Resolution Neutron Powder Diffraction and Solid State NMR. *J. Chem. Soc., Dalton Trans.* 2002, *10*, 2112−2118.

(68) Chiara, R.; Morana, M.; Malavasi, L. Germanium-Based Halide Perovskites: Materials, Properties, and Applications. *ChemPlusChem.* 2021, *86* (6), 879−888.

(69) Drozdowski, D.; Gągor, A.; Stefańska, D.; Zaręba, J. K.; Fedoruk, K.; Mączka, M.; Sieradzki, A. Three-Dimensional Methyl-hydrazinium Lead Halide Perovskites: Structural Changes and Effects on Dielectric, Linear, and Nonlinear Optical Properties Entailed by the Halide Tuning. *J. Phys. Chem. C* 2022, *126* (3), 1600−1610.

(70) Thiele, G.; Serr, B. R. Crystal Structure of Trimethylammonium Tribromostannate(II), (CH3)3NHSnBr3. *Z. Kristallogr.* 1996, *211* (1), 46−46.

(71) Yamada, K.; Isobe, K.; Okuda, T.; Furukawa, Y. Successive Phase Transitions and High Ionic Conductivity of Trichlorogerma-nate (II) Salts as Studied by 35C1 NQR and Powder X-Ray Diffraction. *Z. Für Naturforschung A* 1994, *49* (1−2), 258−266.

(72) Möller, A.; Felsche, J. Crystal Data for N(CH3)4GeCl3. *J. Appl. Crystallogr.* 1979, *12* (6), 617−618.

(73) Mączka, M.; Ptak, M.; Gągor, A.; Zaręba, J. K.; Liang, X.; Balčiūnas, S.; Semenikhin, O. A.; Kucheriv, O. I.; Gural'skiy, I. A.; Shova, S.; Walsh, A.; Banys, J.; Šimėnas, M. Phase Transitions, Dielectric Response, and Nonlinear Optical Properties of Aziridinium Lead Halide Perovskites. *Chem. Mater.* 2023, *35* (22), 9725−9738.

(74) Abhervé, A.; Mercier, N.; Kumar, A.; Das, T. K.; Even, J.; Katan, C.; Kepenekian, M. Chirality Versus Symmetry: Electron's Spin Selectivity in Non-Polar Chiral Lead-Bromide Perovskites. *Adv. Mater.* 2023, *35*, No. 2305784.

(75) Berastegui, P.; Hull, S.; Eriksson, S.-G. A Low-Temperature Structural Phase Transition in CsPbF3. *J. Phys.: Condens. Matter* 2001, *13* (22), 5077.

(76) Ayub, G.; Rauf, A.; Husain, M.; Algahtani, A.; Tirth, V.; Al-Mughanam, T.; Alghtani, A. H.; Sfina, N.; Rahman, N.; Sohail, M.; Khan, R.; Azzouz-Rached, A.; Khan, A.; Al-Shaalan, N. H.; Alharthi, S.; Alharthy, S. A.; Amin, M. A. Investigating the Physical Properties of Thallium-Based Ternary TlXF3 (X = Be, Sr) Fluoroperovskite Compounds for Prospective Applications. *ACS Omega* 2023, *8* (20), 17779−17787.

(77) Yang, R. X.; Skelton, J. M.; da Silva, E. L.; Frost, J. M.; Walsh, A. Spontaneous Octahedral Tilting in the Cubic Inorganic Cesium Halide Perovskites CsSnX3 and CsPbX3 (X = F, Cl, Br, I). *J. Phys. Chem. Lett.* 2017, *8* (19), 4720−4726.

(78) Selmani, Y.; Labrim, H.; Mouatassime, M.; Bahmad, L. Structural, Optoelectronic and Thermoelectric Properties of Cs-Based Fluoroperovskites CsMF3 (M= Ge, Sn or Pb). *Mater. Sci. Semicond. Process.* 2022, *152*, No. 107053.

(79) Thao Tran, T.; Shiv Halasyamani, P. Synthesis and Character-ization of ASnF3 (A = Na+, K+, Rb+, Cs+). *J. Solid State Chem.* 2014, *210* (1), 213−218.

(80) Andersen, N. H.; Kjems, J. K.; Hayes, W. Ionic Conductivity of the Perovskites NaMgF3, KMgF3, KMgK3 and KZnF3 at High Temperatures. *Solid State Ion.* 1985, *17* (2), 143−145.

(81) Simenas, M.; Gagor, A.; Banys, J.; Maczka, M. Phase Transitions and Dynamics in Mixed Three- and Low-Dimensional Lead Halide Perovskites. *Chem. Rev.* 2024, *124* (5), 2281−2326.

(82) Wolf, N. R.; Connor, B. A.; Slavney, A. H.; Karunadasa, H. I. Doubling the Stakes: The Promise of Halide Double Perovskites. *Angew. Chem., Int. Ed.* 2021, *60* (30), 16264−16278.

(83) Retuerto, M.; Emge, T.; Hadermann, J.; Stephens, P. W.; Li, M. R.; Yin, Z. P.; Croft, M.; Ignatov, A.; Zhang, S. J.; Yuan, Z.; Jin, C.; Simonson, J. W.; Aronson, M. C.; Pan, A.; Basov, D. N.; Kotliar, G.; Greenblatt, M. Synthesis and Properties of Charge-Ordered Thallium Halide Perovskites, CsTl+0.5Tl3 + 0.5 × 3 (X = F or Cl): Theoretical Precursors for Superconductivity? *Chem. Mater.* 2013, *25* (20), 4071−4079.

(84) Elliott, N.; Pauling, L. The Crystal Structure of Cesium Aurous Auric Chloride, Cs2AuAuCl6, and Cesium Argentous Auric Chloride, Cs2AgAuCl6. *J. Am. Chem. Soc.* 1938, *60* (8), 1846−1851.

(85) Slavney, A. H.; Hu, T.; Lindenberg, A. M.; Karunadasa, H. I. A Bismuth-Halide Double Perovskite with Long Carrier Recombination Lifetime for Photovoltaic Applications. *J. Am. Chem. Soc.* 2016, *138* (7), 2138−2141.

(86) Volonakis, G.; Haghighirad, A. A.; Milot, R. L.; Sio, W. H.; Filip, M. R.; Wenger, B.; Johnston, M. B.; Herz, L. M.; Snaith, H. J.; Giustino, F. Cs2InAgCl6: A New Lead-Free Halide Double Perovskite with Direct Band Gap. *J. Phys. Chem. Lett.* 2017, *8* (4), 772−778.

(87) Tran, T. T.; Panella, J. R.; Chamorro, J. R.; Morey, J. R.; McQueen, T. M. Designing Indirect−Direct Bandgap Transitions in Double Perovskites. *Mater. Horiz* 2017, *4* (4), 688−693.

(88) Slavney, A. H.; Leppert, L.; Saldivar Valdes, A.; Bartesaghi, D.; Savenije, T. J.; Neaton, J. B.; Karunadasa, H. I. Small-Band-Gap Halide Double Perovskites. *Angew. Chem., Int. Ed.* 2018, *57* (39), 12765−12770.

(89) Deng, Z.; Wei, F.; Sun, S.; Kieslich, G.; Cheetham, A. K.; Bristowe, P. D. Exploring the Properties of Lead-Free Hybrid Double Perovskites Using a Combined Computational-Experimental Ap-proach. *J. Mater. Chem. A* 2016, *4* (31), 12025−12029.

(90) Ke, W.; Stoumpos, C. C.; Spanopoulos, I.; Mao, L.; Chen, M.; Wasielewski, M. R.; Kanatzidis, M. G. Efficient Lead-Free Solar Cells Based on Hollow {en}MASnI3 Perovskites. *J. Am. Chem. Soc.* 2017, *139* (41), 14800−14806.

(91) Spanopoulos, I.; Ke, W.; Stoumpos, C. C.; Schueller, E. C.; Kontsevoi, O. Y.; Seshadri, R.; Kanatzidis, M. G. Unraveling the Chemical Nature of the 3D "Hollow" Hybrid Halide Perovskites. *J. Am. Chem. Soc.* 2018, *140* (17), 5728−5742.

(92) Spanopoulos, I.; Hadar, I.; Ke, W.; Guo, P.; Mozur, E. M.; Morgan, E.; Wang, S.; Zheng, D.; Padgaonkar, S.; Manjunatha Reddy, G. N.; Weiss, E. A.; Hersam, M. C.; Seshadri, R.; Schaller, R. D.; Kanatzidis, M. G. Tunable Broad Light Emission from 3D "Hollow" Bromide Perovskites through Defect Engineering. *J. Am. Chem. Soc.* 2021, *143* (18), 7069−7080.

(93) Li, X.; Kepenekian, M.; Li, L.; Dong, H.; Stoumpos, C. C.; Seshadri, R.; Katan, C.; Guo, P.; Even, J.; Kanatzidis, M. G. Tolerance Factor for Stabilizing 3D Hybrid Halide Perovskitoids Using Linear Diammonium Cations. *J. Am. Chem. Soc.* 2022, *144* (9), 3902−3912.

(94) Baikie, T.; Barrow, N. S.; Fang, Y.; Keenan, P. J.; Slater, P. R.; Piltz, R. O.; Gutmann, M.; Mhaisalkar, S. G.; White, T. J. A Combined Single Crystal Neutron/X-Ray Diffraction and Solid-State Nuclear Magnetic Resonance Study of the Hybrid Perovskites CH3NH3PbX3 (X = I, Br and Cl). *J. Mater. Chem. A* 2015, *3* (17), 9298−9307.

(95) Bakulin, A. A.; Selig, O.; Bakker, H. J.; Rezus, Y. L. A.; Müller, C.; Glaser, T.; Lovrincic, R.; Sun, Z.; Chen, Z.; Walsh, A.; Frost, J. M.; Jansen, T. L. C. Real-Time Observation of Organic Cation Reorientation in Methylammonium Lead Iodide Perovskites. *J. Phys. Chem. Lett.* 2015, *6* (18), 3663−3669.

(96) Xu, Q.; Eguchi, T.; Nakayama, H.; Nakamura, N.; Kishita, M. Molecular Motions and Phase Transitions in Solid CH3NH3PbX3 (X = C1, Br, I) as Studied by NMR and NQR. *Zeitschrift für Naturforschung A* 1991, *46* (3), 240−246.

(97) Leguy, A. M. A.; Frost, J. M.; McMahon, A. P.; Sakai, V. G.; Kockelmann, W.; Law, C.; Li, X.; Foglia, F.; Walsh, A.; O'Regan, B. C.; Nelson, J.; Cabral, J. T.; Barnes, P. R. F. The Dynamics of Methylammonium Ions in Hybrid Organic−Inorganic Perovskite Solar Cells. *Nat. Commun.* 2015, *6* (1), 7124.

(98) Taylor, V. C. A.; Tiwari, D.; Duchi, M.; Donaldson, P. M.; Clark, I. P.; Fermin, D. J.; Oliver, T. A. A. Investigating the Role of the Organic Cation in Formamidinium Lead Iodide Perovskite Using Ultrafast Spectroscopy. *J. Phys. Chem. Lett.* 2018, *9* (4), 895−901.

(99) Fabini, D. H.; Siaw, T. A.; Stoumpos, C. C.; Laurita, G.; Olds, D.; Page, K.; Hu, J. G.; Kanatzidis, M. G.; Han, S.; Seshadri, R. Universal Dynamics of Molecular Reorientation in Hybrid Lead Iodide Perovskites. *J. Am. Chem. Soc.* 2017, *139* (46), 16875−16884.

(100) Mozur, E. M.; Neilson, J. R. Cation Dynamics in Hybrid Halide Perovskites. *Annu. Rev. Mater. Res.* 2021, *51*, 269−291.

(101) Weadock, N. J.; Sterling, T. C.; Vigil, J. A.; Gold-Parker, A.; Smith, I. C.; Ahammed, B.; Krogstad, M. J.; Ye, F.; Voneshen, D.; Gehring, P. M.; Rappe, A. M.; Steinrück, H.-G.; Ertekin, E.; Karunadasa, H. I.; Reznik, D.; Toney, M. F. The Nature of Dynamic Local Order in CH3NH3PbI3 and CH3NH3PbBr3. *Joule* **2023**, *7* (5), 1051–1066.

(102) Li, Z.; Yang, M.; Park, J.-S.; Wei, S.-H.; Berry, J. J.; Zhu, K. Stabilizing Perovskite Structures by Tuning Tolerance Factor: Formation of Formamidinium and Cesium Lead Iodide Solid-State Alloys. *Chem. Mater.* **2016**, *28* (1), 284–292.

(103) Vigil, J. A.; Hazarika, A.; Luther, J. M.; Toney, M. F. FAxCs1−xPbI3 Nanocrystals: Tuning Crystal Symmetry by A-Site Cation Composition. *ACS Energy Lett.* **2020**, *5* (8), 2475–2482.

(104) Hazarika, A.; Zhao, Q.; Gaulding, E. A.; Christians, J. A.; Dou, B.; Marshall, A. R.; Moot, T.; Berry, J. J.; Johnson, J. C.; Luther, J. M. Perovskite Quantum Dot Photovoltaic Materials beyond the Reach of Thin Films: Full-Range Tuning of A-Site Cation Composition. *ACS Nano* **2018**, *12* (10), 10327–10337.

(105) Šimėnas, M.; Balčiūnas, S.; Gągor, A.; Pieniążek, A.; Tolborg, K.; Kinka, M.; Klimavicius, V.; Svirskas, Š.; Kalendra, V.; Ptak, M.; Szewczyk, D.; Herman, A. P.; Kudrawiec, R.; Sieradzki, A.; Grigalaitis, R.; Walsh, A.; Mączka, M.; Banys, J. Mixology of MA1−xEAxPbI3 Hybrid Perovskites: Phase Transitions, Cation Dynamics, and Photoluminescence. *Chem. Mater.* **2022**, *34* (22), 10104–10112.

(106) Mozur, E. M.; Hope, M. A.; Trowbridge, J. C.; Halat, D. M.; Daemen, L. L.; Maughan, A. E.; Prisk, T. R.; Grey, C. P.; Neilson, J. R. Cesium Substitution Disrupts Concerted Cation Dynamics in Formamidinium Hybrid Perovskites. *Chem. Mater.* **2020**, *32* (14), 6266–6277.

(107) Šimėnas, M.; Balčiūnas, S.; Svirskas, Š.; Kinka, M.; Ptak, M.; Kalendra, V.; Gągor, A.; Szewczyk, D.; Sieradzki, A.; Grigalaitis, R.; Walsh, A.; Mączka, M.; Banys, J. Phase Diagram and Cation Dynamics of Mixed MA1−xFAxPbBr3 Hybrid Perovskites. *Chem. Mater.* **2021**, *33* (15), 5926–5934.

(108) Mozur, E. M.; Maughan, A. E.; Cheng, Y.; Huq, A.; Jalarvo, N.; Daemen, L. L.; Neilson, J. R. Orientational Glass Formation in Substituted Hybrid Perovskites. *Chem. Mater.* **2017**, *29* (23), 10168–10177.

(109) Akkerman, Q. A.; D'Innocenzo, V.; Accornero, S.; Scarpellini, A.; Petrozza, A.; Prato, M.; Manna, L. Tuning the Optical Properties of Cesium Lead Halide Perovskite Nanocrystals by Anion Exchange Reactions. *J. Am. Chem. Soc.* **2015**, *137* (32), 10276–10281.

(110) Domanski, K.; Roose, B.; Matsui, T.; Saliba, M.; Turren-Cruz, S.-H.; Correa-Baena, J.-P.; Carmona, C. R.; Richardson, G.; Foster, J. M.; De Angelis, F.; Ball, J. M.; Petrozza, A.; Mine, N.; Nazeeruddin, M. K.; Tress, W.; Grätzel, M.; Steiner, U.; Hagfeldt, A.; Abate, A. Migration of Cations Induces Reversible Performance Losses over Day/Night Cycling in Perovskite Solar Cells. *Energy Env. Sci.* **2017**, *10* (2), 604–613.

(111) Kim, J. Y.; Lee, J.-W.; Jung, H. S.; Shin, H.; Park, N.-G. High-Efficiency Perovskite Solar Cells. *Chem. Rev.* **2020**, *120* (15), 7867–7918.

(112) Zhu, H.; Teale, S.; Lintangpradipto, M. N.; Mahesh, S.; Chen, B.; McGehee, M. D.; Sargent, E. H.; Bakr, O. M. Long-Term Operating Stability in Perovskite Photovoltaics. *Nat. Rev. Mater.* **2023**, *8* (9), 569–586.

(113) Byranvand, M. M.; Otero-Martínez, C.; Ye, J.; Zuo, W.; Manna, L.; Saliba, M.; Hoye, R. L. Z.; Polavarapu, L. Recent Progress in Mixed A-Site Cation Halide Perovskite Thin-Films and Nanocrystals for Solar Cells and Light-Emitting Diodes. *Adv. Opt. Mater.* **2022**, *10* (14), No. 2200423.

(114) Fu, Y.; Hautzinger, M. P.; Luo, Z.; Wang, F.; Pan, D.; Aristov, M. M.; Guzei, I. A.; Pan, A.; Zhu, X.; Jin, S. Incorporating Large A Cations into Lead Iodide Perovskite Cages: Relaxed Goldschmidt Tolerance Factor and Impact on Exciton−Phonon Interaction. *ACS Cent. Sci.* **2019**, *5* (8), 1377–1386.

(115) Hautzinger, M. P.; Pan, D.; Pigg, A. K.; Fu, Y.; Morrow, D. J.; Leng, M.; Kuo, M.-Y.; Spitha, N.; Lafayette, D. P. I.; Kohler, D. D.; Wright, J. C.; Jin, S. Band Edge Tuning of Two-Dimensional

Ruddlesden−Popper Perovskites by A Cation Size Revealed through Nanoplates. *ACS Energy Lett.* **2020**, *5* (5), 1430–1437.

(116) Li, X.; Fu, Y.; Pedesseau, L.; Guo, P.; Cuthriell, S.; Hadar, I.; Even, J.; Katan, C.; Stoumpos, C. C.; Schaller, R. D.; Harel, E.; Kanatzidis, M. G. Negative Pressure Engineering with Large Cage Cations in 2D Halide Perovskites Causes Lattice Softening. *J. Am. Chem. Soc.* **2020**, *142* (26), 11486–11496.

(117) Fu, Y. Stabilization of Metastable Halide Perovskite Lattices in the 2D Limit. *Adv. Mater.* **2022**, *34* (9), No. 2108556.

(118) Yan, J.; Zhang, W.; Geng, S.; Qiu, C.; Chu, Y.; Meng, R.; Zeng, P.; Liu, M.; Xiao, Z.; Hu, Y. Electronic State Modulation by Large A-Site Cations in Quasi-Two-Dimensional Organic−Inorganic Lead Halide Perovskites. *Chem. Mater.* **2023**, *35* (1), 289–294.

(119) Xu, Z.; Li, Y.; Liu, X.; Ji, C.; Chen, H.; Li, L.; Han, S.; Hong, M.; Luo, J.; Sun, Z. Highly Sensitive and Ultrafast Responding Array Photodetector Based on a Newly Tailored 2D Lead Iodide Perovskite Crystal. *Adv. Opt. Mater.* **2019**, *7* (11), No. 1900308.

(120) Wang, Y.; Liu, X.; Li, L.; Ji, C.; Sun, Z.; Han, S.; Tao, K.; Luo, J. (C6H13NH3)2(NH2CHNH2)Pb2I7: A Two-Dimensional Bilayer Inorganic−Organic Hybrid Perovskite Showing Photodetecting Behavior. *Chem. Asian J.* **2019**, *14* (9), 1530–1534.

(121) Yang, T.; Li, Y.; Han, S.; Liu, X.; Xu, Z.; Li, M.; Wang, J.; Ma, Y.; Luo, J.; Sun, Z. Exploiting Two-Dimensional Hybrid Perovskites Incorporating Secondary Amines for High-Performance Array Photodetection. *J. Mater. Chem. C* **2020**, *8* (37), 12848–12853.

(122) Mihalyi-Koch, W.; Guo, S.; Dai, Z.; Pan, D.; Lafayette, D. P., II; Scheeler, J. M.; Sanders, K. M.; Teat, S. J.; Wright, J. C.; Lü, X.; Rappe, A. M.; Jin, S. Revealing Hidden Non-Centrosymmetry in Globally Centrosymmetric 2D Halide Perovskites. *Chem.* **2024**, *10* (7), 2180–2195.

(123) Mihalyi-Koch, W.; Folpini, G.; Roy, C. R.; Kaiser, W.; Wu, C.-S.; Sanders, K. M.; Guzei, I. A.; Wright, J. C.; De Angelis, F.; Cortecchia, D.; Petrozza, A.; Jin, S. Tuning Structure and Excitonic Properties of 2D Ruddlesden−Popper Germanium, Tin, and Lead Iodide Perovskites via Interplay between Cations. *J. Am. Chem. Soc.* **2023**, *145* (51), 28111–28123.

(124) Fu, Y.; Jiang, X.; Li, X.; Traore, B.; Spanopoulos, I.; Katan, C.; Even, J.; Kanatzidis, M. G.; Harel, E. Cation Engineering in Two-Dimensional Ruddlesden−Popper Lead Iodide Perovskites with Mixed Large A-Site Cations in the Cages. *J. Am. Chem. Soc.* **2020**, *142* (8), 4008–4021.

(125) Han, S.; Liu, X.; Liu, Y.; Xu, Z.; Li, Y.; Hong, M.; Luo, J.; Sun, Z. High-Temperature Antiferroelectric of Lead Iodide Hybrid Perovskites. *J. Am. Chem. Soc.* **2019**, *141* (32), 12470–12474.

(126) Han, S.; Li, L.; Ji, C.; Liu, X.; Wang, G.-E.; Xu, G.; Sun, Z.; Luo, J. Visible-Photoactive Perovskite Ferroelectric-Driven Self-Powered Gas Detection. *J. Am. Chem. Soc.* **2023**, *145* (23), 12853–12860.

(127) Liu, Y.; Guo, W.; Hua, L.; Zeng, X.; Yang, T.; Fan, Q.; Ma, Y.; Gao, C.; Sun, Z.; Luo, J. Giant Polarization Sensitivity via the Anomalous Photovoltaic Effect in a Two-Dimensional Perovskite Ferroelectric. *J. Am. Chem. Soc.* **2023**, *145* (29), 16193–16199.

(128) Wu, Z.; Ji, C.; Li, L.; Kong, J.; Sun, Z.; Zhao, S.; Wang, S.; Hong, M.; Luo, J. Alloying N-Butylamine into CsPbBr3 To Give a Two-Dimensional Bilayered Perovskite Ferroelectric Material. *Angew. Chem., Int. Ed.* **2018**, *57* (27), 8140–8143.

(129) Forlano, K. M.; Roy, C. R.; Mihalyi-Koch, W.; Hossain, T.; Sanders, K.; Guzei, I.; Graham, K. R.; Wright, J. C.; Jin, S. High Layer Number (n = 1−6) 2D Ruddlesden−Popper Lead Bromide Perovskites: Nanosheets, Crystal Structure, and Optoelectronic Properties. *ACS Mater. Lett.* **2023**, *5* (11), 2913–2921.

(130) Li, L.; Liu, X.; Li, Y.; Xu, Z.; Wu, Z.; Han, S.; Tao, K.; Hong, M.; Luo, J.; Sun, Z. Two-Dimensional Hybrid Perovskite-Type Ferroelectric for Highly Polarization-Sensitive Shortwave Photodetection. *J. Am. Chem. Soc.* **2019**, *141* (6), 2623–2629.

(131) Li, L.; Shang, X.; Wang, S.; Dong, N.; Ji, C.; Chen, X.; Zhao, S.; Wang, J.; Sun, Z.; Hong, M.; Luo, J. Bilayered Hybrid Perovskite Ferroelectric with Giant Two-Photon Absorption. *J. Am. Chem. Soc.* **2018**, *140* (22), 6806–6809.

(132) Mao, L.; Wu, Y.; Stoumpos, C. C.; Traore, B.; Katan, C.; Even, J.; Wasielewski, M. R.; Kanatzidis, M. G. Tunable White-Light Emission in Single-Cation-Templated Three-Layered 2D Perovskites (CH3CH2NH3)4Pb3Br10−xClx. *J. Am. Chem. Soc.* **2017**, *139* (34), 11956−11963.

(133) Ji, C.; Wang, S.; Wang, Y.; Chen, H.; Li, L.; Sun, Z.; Sui, Y.; Wang, S.; Luo, J. 2D Hybrid Perovskite Ferroelectric Enables Highly Sensitive X-Ray Detection with Low Driving Voltage. *Adv. Funct. Mater.* **2020**, *30* (5), No. 1905529.

(134) Peng, Y.; Bie, J.; Liu, X.; Li, L.; Chen, S.; Fa, W.; Wang, S.; Sun, Z.; Luo, J. Acquiring High-TC Layered Metal Halide Ferroelectrics via Cage-Confined Ethylamine Rotators. *Angew. Chem., Int. Ed.* **2021**, *60* (6), 2839−2843.

(135) Liu, Y.; Han, S.; Wang, J.; Ma, Y.; Guo, W.; Huang, X.-Y.; Luo, J.-H.; Hong, M.; Sun, Z. Spacer Cation Alloying of a Homoconformational Carboxylate Trans Isomer to Boost In-Plane Ferroelectricity in a 2D Hybrid Perovskite. *J. Am. Chem. Soc.* **2021**, *143* (4), 2130−2137.

(136) Geselle, M.; Fuess, H. Crystal Structure of Tetrakis-(Ethylammonium) Decachlorotriplumbate(II), (C2H5NH3)-4Pb3Cl10. *Z. Für Krist. - New Cryst. Struct.* **1997**, *212* (1), 241−242.

(137) Li, X.; Dong, H.; Volonakis, G.; Stoumpos, C. C.; Even, J.; Katan, C.; Guo, P.; Kanatzidis, M. G. Ordered Mixed-Spacer 2D Bromide Perovskites and the Dual Role of 1,2,4-Triazolium Cation. *Chem. Mater.* **2022**, *34* (14), 6541−6552.

(138) Li, X.; Cuthriell, S. A.; Bergonzoni, A.; Dong, H.; Traoré, B.; Stoumpos, C. C.; Guo, P.; Even, J.; Katan, C.; Schaller, R. D.; Kanatzidis, M. G. Expanding the Cage of 2D Bromide Perovskites by Large A-Site Cations. *Chem. Mater.* **2022**, *34* (3), 1132−1142.

(139) Fan, Q.; Ma, Y.; Xu, H.; Liu, Y.; Wang, B.; Guo, W.; Hu, X.; Luo, J.; Sun, Z. Acquiring a Newly Tailored 2D Dion−Jacobson Hybrid Perovskite with Large Structural Distortion for Efficient Crystal Array Photodetector. *Adv. Opt. Mater.* **2023**, *11* (2), No. 2202277.

(140) Fu, D.; Jia, W.; Wu, S.; Chang, J.; Chen, Z.; Luo, J. Bilayered Dion−Jacobson Hybrid Perovskite Bulk Single Crystals Constructed with Aromatic Diammonium for Ultraviolet−Visible−Near-Infrared Photodetection. *Chem. Mater.* **2023**, *35* (6), 2541−2548.

(141) Fu, D.; Pan, L.; Ma, Y.; Zhang, Y. Bilayered Dion-Jacobson Lead-Iodine Hybrid Perovskite with Aromatic Spacer for Broadband Photodetection. *Chin. Chem. Lett.* **2024**, No. 109621.

(142) Arya, S.; Mahajan, P.; Gupta, R.; Srivastava, R.; Tailor, N. k.; Satapathi, S.; Sumathi, R. R.; Datt, R.; Gupta, V. A Comprehensive Review on Synthesis and Applications of Single Crystal Perovskite Halides. *Prog. Solid State Chem.* **2020**, *60*, No. 100286.

(143) Buin, A.; Comin, R.; Xu, J.; Ip, A. H.; Sargent, E. H. Halide-Dependent Electronic Structure of Organolead Perovskite Materials. *Chem. Mater.* **2015**, *27* (12), 4405−4412.

(144) Yin, W.-J.; Shi, T.; Yan, Y. Unique Properties of Halide Perovskites as Possible Origins of the Superior Solar Cell Performance. *Adv. Mater.* **2014**, *26* (27), 4653−4658.

(145) Filip, M. R.; Eperon, G. E.; Snaith, H. J.; Giustino, F. Steric Engineering of Metal-Halide Perovskites with Tunable Optical Band Gaps. *Nat. Commun.* **2014**, *5* (1), 5757.

(146) Prasanna, R.; Gold-Parker, A.; Leijtens, T.; Conings, B.; Babayigit, A.; Boyen, H.-G.; Toney, M. F.; McGehee, M. D. Band Gap Tuning via Lattice Contraction and Octahedral Tilting in Perovskite Materials for Photovoltaics. *J. Am. Chem. Soc.* **2017**, *139* (32), 11117−11124.

(147) Valadares, F.; Guilhon, I.; Teles, L. K.; Marques, M. Electronic Structure Panorama of Halide Perovskites: Approximated DFT-1/2 Quasiparticle and Relativistic Corrections. *J. Phys. Chem. C* **2020**, *124* (34), 18390−18400.

(148) Yin, W.-J.; Shi, T.; Yan, Y. Unusual Defect Physics in CH3NH3PbI3 Perovskite Solar Cell Absorber. *Appl. Phys. Lett.* **2014**, *104* (6), No. 063903.

(149) Dai, J.; Fu, Y.; Manger, L. H.; Rea, M. T.; Hwang, L.; Goldsmith, R. H.; Jin, S. Carrier Decay Properties of Mixed Cation Formamidinium−Methylammonium Lead Iodide Perovskite [HC-(NH2)2]1−x[CH3NH3]xPbI3 Nanorods. *J. Phys. Chem. Lett.* **2016**, *7* (24), 5036−5043.

(150) Guo, S.; Zhao, Y.; Bu, K.; Fu, Y.; Luo, H.; Chen, M.; Hautzinger, M. P.; Wang, Y.; Jin, S.; Yang, W.; Lü, X. Pressure-Suppressed Carrier Trapping Leads to Enhanced Emission in Two-Dimensional Perovskite (HA)2(GA)Pb2I7. *Angew. Chem., Int. Ed.* **2020**, *59* (40), 17533−17539.

(151) Guo, S.; Mihalyi-Koch, W.; Mao, Y.; Li, X.; Bu, K.; Hong, H.; Hautzinger, M. P.; Luo, H.; Wang, D.; Gu, J.; Zhang, Y.; Zhang, D.; Hu, Q.; Ding, Y.; Yang, W.; Fu, Y.; Jin, S.; Lü, X. Exciton Engineering of 2D Ruddlesden−Popper Perovskites by Synergistically Tuning the Intra and Interlayer Structures. *Nat. Commun.* **2024**, *15* (1), 3001.

(152) Xu, F.; Zou, Y.; Dai, Y.; Li, M.; Li, Z. Halide Perovskites and High-Pressure Technologies: A Fruitful Encounter. *Mater. Chem. Front.* **2023**, *7* (11), 2102−2119.

(153) Jin, S. Can We Find the Perfect A-Cations for Halide Perovskites? *ACS Energy Lett.* **2021**, *6* (9), 3386−3389.

(154) Manzi, M.; Pica, G.; De Bastiani, M.; Kundu, S.; Grancini, G.; Saidaminov, M. I. Ferroelectricity in Hybrid Perovskites. *J. Phys. Chem. Lett.* **2023**, *14* (14), 3535−3552.

(155) Zhou, Y.; Huang, Y.; Xu, X.; Fan, Z.; Khurgin, J. B.; Xiong, Q. Nonlinear Optical Properties of Halide Perovskites and Their Applications. *Appl. Phys. Rev.* **2020**, *7* (4), No. 041313.

(156) Findik, G.; Biliroglu, M.; Seyitliyev, D.; Mendes, J.; Barrette, A.; Ardekani, H.; Lei, L.; Dong, Q.; So, F.; Gundogdu, K. High-Temperature Superfluorescence in Methyl Ammonium Lead Iodide. *Nat. Photonics* **2021**, *15* (9), 676−680.

(157) Kaplan, A. E. K.; Krajewska, C. J.; Proppe, A. H.; Sun, W.; Sverko, T.; Berkinsky, D. B.; Utzat, H.; Bawendi, M. G. Hong−Ou−Mandel Interference in Colloidal CsPbBr3 Perovskite Nanocrystals. *Nat. Photonics* **2023**, *17* (9), 775−780.